A COMPUTATIONAL MODEL TO INVESTIGATE THE INFLUENCE OF V1 CELL PROPERTIES AND TOPOGRAPHIC ORGANIZATION ON V2 RESPONSE TO ILLUSORY CONTOURS, WITH APPLICATIONS IN THE STUDY OF CORTICAL INJURIES IN THE PRIMARY VISUAL CORTEX

Amelia Cohen

A dissertation submitted to the faculty of the University of North Carolina at Chapel Hill in partial fulfillment of the requirements for the degree of Doctor of Philosophy in the Department of Physics and Astronomy.

Chapel Hill
2011

Approved by:

Paul Tiesinga

David Hubel

Thomas Clegg

Michael Falvo

Amy Oldenburg

ABSTRACT

AMELIA COHEN: A computational model to investigate the influence of V1 cell properties and topographic organization on V2 response to illusory contours, with applications in the study of cortical injuries in the primary visual cortex

(Under the direction of Paul Tiesinga)

I present a model capable of illusory contour detection. Unlike previous models, this model uses a realistic topographic organization of the orientation preferences of cells in the primary visual cortex. I show that using a feed-forward mechanism, this model can accomplish illusory contour detection at the level of V2 even with a non-uniform distribution of orientation preferences amongst simple and complex cells. The model is applied to the study of the properties of V2 cells that respond to illusory contours. I show that 1) inducer spacing preference depends directly on the receptive field width of simple cells in the primary visual cortex, 2) the shift in the orientation tuning peak as a function of inducer angle relative to illusory contour orientation is determined by the distribution of end-stopped cell orientation preferences in the presynaptic input to the V2 cell, and 3) the contrast response function of V2 cells increases more rapidly for real contours than for illusory contours.

I also use the model to study the consequences of a primary visual cortex lesion on visual function. I show that for small lesions, response degradation for neurons

downstream from the injured area increases linearly with the size of the damage. Using an additional layer of classifier units as a proxy for neural correlates of higher visual functions, I characterize the extent to which recovery of visual function is possible following cortical injury. I show that while both spontaneous and training-induced recovery can lead to restoration of visual function, spontaneous recovery is more effective, and under certain conditions can restore visual function to pre-lesion levels.

For Calin.

ACKNOWLEDGEMENTS

First, I would like to thank my committee for their patience and insight, in particular my adviser Paul Tiesinga. I would also especially like to thank David Hubel, who was a constant source of inspiration both through his work and over many a cup of tea.

I would also like to thank my family: my parents, my sister and brother, and my husband who all supported me through many years of hard work.

Furthermore, I would like to thank the many friends and colleagues who have provided a critical eye, or a sympathetic ear, or a good laugh when it was most needed.

Finally, I would like to thank the physics department at James Madison University, who provided me with the foundation I needed to complete this work.

TABLE OF CONTENTS

LIST OF TABLES

LIST OF FIGURES

Chapter I

Introduction

The brain enables us to perceive our environment by taking in vast quantities of information and processing it through thousands of computations performed every second. Current experimental techniques are able to provide only a small glimpse into the neural activity behind this processing, yet the amount of data collected thus far is overwhelming. We are faced with both too little information and too much: There are still many questions about neural circuitry and behavior that cannot be answered, but we also face difficulties in making sense of the vast quantities of data already available. Computational modeling is a powerful tool that enables us to integrate the data at hand into mechanisms that explain the functions of the brain and at the same time allows us to fill in the gaps that cannot be addressed by current experimental techniques.

One of the most important functions of the visual system is the separation of a visual scene into distinct objects. This is far from trivial, as the information the brain receives from the retina is a two dimensional representation of a three dimensional world. As a consequence, objects are generally separated from the background by making use of physical discontinuities in the image (gradient in color or contrast) to define their boundaries (Albright and Stoner 2002). Changes in illumination, shadows cast by light

sources or backgrounds of similar color and texture to the object can diminish or eliminate such discontinuities, yet we are able to correctly detect objects boundaries even under such circumstances. Contours perceived in the absence of color or contrast gradients are called illusory contours and they play an important role in the identification of object boundaries (Nieder 2002, Albright and Stoner 2002). The neural processes governing the response of the visual cortex to such contours is still not fully understood, and constitutes the object of the present work.

This thesis uses a firing rate model to investigate the mechanism of illusory contour detection. The model allows us to advance explanations for observed properties of cells in the V2 area of the visual cortex, and as a practical application, it can be used to assess and characterize the effects of a cortical injury in the V1 area on higher visual functions.

Chapter II presents the necessary neurobiology background for the thesis. Beginning with the eye and progressing to the visual cortex, it focuses on the structure and function of the visual areas, particularly those necessary for early processing, and explains terminology necessary for understanding this work. It also discusses experimental techniques that are used in neurobiology, with a focus on illusory contour detection, and discusses previous models of illusory contour detection.

Chapter III describes the model in detail both at the level of individual cell properties and at the level of neural circuitry. It explains the receptive field characteristics of each cell type, and how appropriate connections build cells with progressively more complex response properties. We show that the model cells reproduce

experimentally observed properties at each level, and that the model pattern cells respond to illusory contours.

In Chapter IV we use the model to study several properties of illusory contour detection. These include the effect of a realistic presynaptic orientation map, inducer spacing preference, inducer angle dependence, and contrast response function. We find the following: 1) Illusory contour detection can be achieved in V2 using a realistic V1 orientation preference map, which can account in part for the variability measured experimentally, 2) Inducer spacing preference is dependent on the receptive field width of presynaptic simple cells, 3) Response of individual cells to illusory contours with non-orthogonal inducers is determined by the distribution of orientation preferences in the presynaptic input, and 4) The contrast response function increases more slowly for illusory contours than for real contours. Additionally, the model is used to estimate the relationship between the extent of a V1 cortical injury and the V2 responses to real and illusory contours.

In Chapter V we apply the model to the study of V1 cortical lesions and their impact on higher order visual function. We investigate possible mechanisms for recovery of functionality in higher cortical areas using a simple figure-ground segregation paradigm as a proxy for higher visual functions. We find that the likelihood of recovering functionality is significantly higher when retraining is performed immediately after the injury versus several months later.

In Chapter VI we discuss the results and possible implications.

Chapter II

Neurobiological Background

Neurobiology is the study of the nervous system. The nervous system controls most of the major functions in the body, and is divided into two main components: the central nervous system (CNS), which consists of the brain and the spinal cord, and the peripheral nervous system (PNS), which innervates the skin, joints and muscles that are controlled voluntarily, as well as the internal organs, blood vessels and glands. The central nervous system, specifically the brain, is the main focus of this work and will be discussed here in greater detail.

2.1 The Brain: an Overview

The brain is comprised of the cerebrum, the cerebellum and the brain stem. The cerebrum, where most neural processing takes place, contains the cerebral cortex, the limbic system (which includes the thalamus), and the basal ganglia. The cerebral cortex is divided into four lobes: frontal, parietal, temporal, and occipital. These different regions of the brain are responsible for different functions, and are further subdivided into more specialized regions. The localization of brain function is one of the fundamental

principles of neuroscience. This thesis focuses on functions of the occipital lobe, which is concerned with vision.

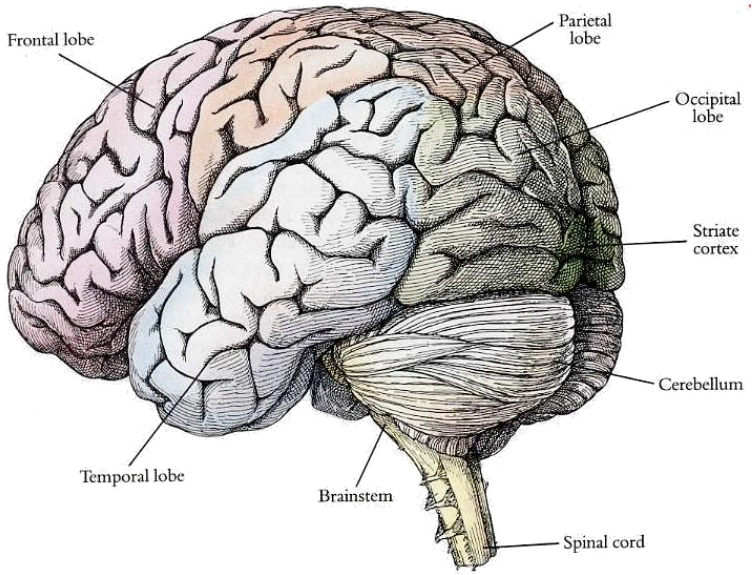

Figure 2.1 A schematic of the brain. Adapted from Eye, Brain and Vision (Hubel 1995).

The neuron is the fundamental processing unit of the cortex. The structure of a neuron includes a cell body, or soma, and projections known as axons and dendrites. Most neurons have a single axon and can have numerous dendritic branches. At the end of each axon are connections to other neurons known as synapses. A synapse is located between the first (presynaptic) cell's axon and the second (postsynaptic) cell's axon, dendrite, or soma. Release, diffusion, and subsequent binding to receptors of neurotransmitters at these synapses is responsible for propagation of information within the cortex.

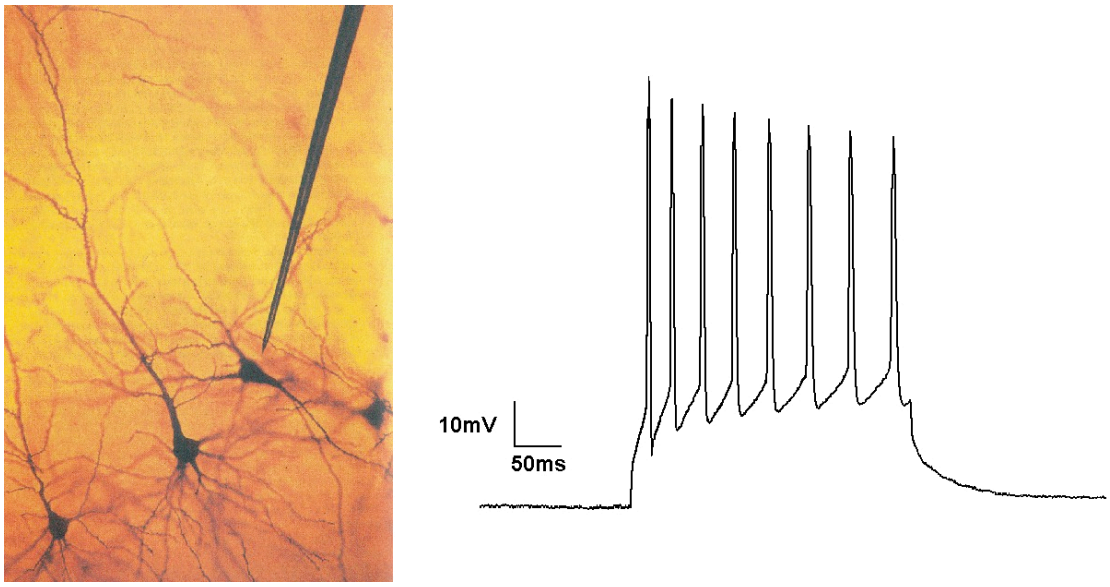

Figure 2.2 The neuron. Left: An image from the monkey visual cortex using Golgi staining, adapted from Eye Brain and Vision (Hubel 1995). Right: Action potentials recorded from a single neuron.

A cell's voltage relative to its surroundings is known as the *membrane potential*. When there is no neural activity, the membrane potential is at the *resting potential*, typically in the range of -70 mV (Shepherd 2009). A neuron's membrane potential is affected by the concentration of various ions within the neuron relative to the concentration of ions in the surrounding area, and by the presence of neurotransmitters received from presynaptic cells. When a neuron becomes sufficiently depolarized (that is, when its voltage is sufficiently high relative to the resting potential), a rapid change in voltage known as a *spike* or *action potential* occurs. When a cell produces an action potential, the change in voltage originates in the soma and propagates along the axon. As the action potential travels along the axon, ion channels open and close along the surface,

allowing charged ions to pass through the cell membrane and change the cell's voltage. A typical action potential involves sodium ions entering the cell and causing the voltage to increase, followed by potassium ions flowing out and causing the voltage to return to the resting potential. Other ions, including chloride and calcium, can also be involved. When a cell produces an action potential, it releases neurotransmitters at its synapses with downstream neurons, which increases or decreases the probability that the postsynaptic neuron will produce an action potential, depending on the type of neurotransmitter released. The rate and timing with which a cell produces action potentials is how neurons transmit information through the brain.

2.2 The Visual System

The visual system is responsible for translating light signals received by the eye into electrical signals that the brain can use to transmit and process information. Light first enters the eye in the form of photons converging on the retina. The retina converts these light signals into electrical signals and transmits them to the thalamus, specifically to the lateral geniculate nucleus (LGN). The thalamus is responsible for collecting diverse sensory information and transmitting it to the various areas of the cortex. In the case of visual processing, the LGN transmits information to, and receives feedback from, the primary visual cortex, where all higher level visual processing takes place.

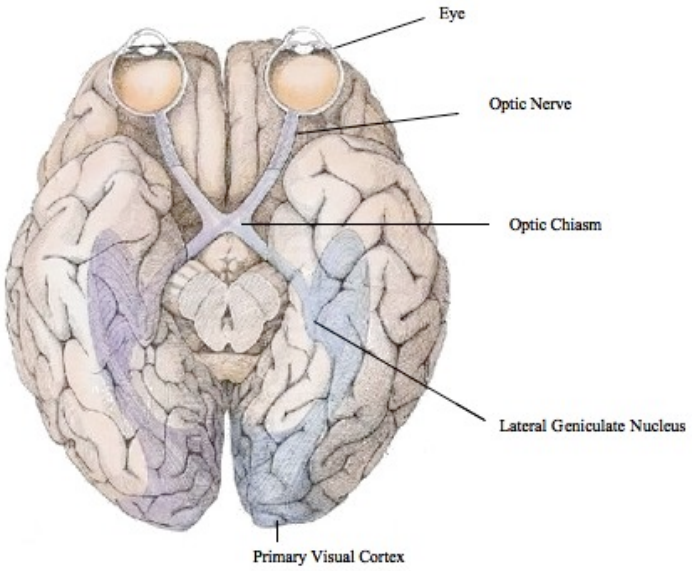

Figure 2.3 A schematic of the visual system. This figure shows the visual pathway. Information enters through the eye, travels along the optic nerve, and crosses at the optic chiasm before entering the lateral geniculate nucleus. From there, it is transmitted to the primary visual cortex. Adapted from Eye, Brain and Vision (Hubel 1995).

2.2.1 The Eye

The eye is the first stage of visual processing. Visual information enters the eye in the form of light through the cornea. It is then further refracted by the lens, which expands or contracts to bring the outer image into focus on the retina. The image projected on the retina is an inverted image of the visual field.

The retina consists of three layers of cells. The first stage of retinal processing involves of photoreceptors, which are divided into rods and cones. These cells contain rhodopsin, a pigment that absorbs incoming photons and allows the cell to transform the incoming light into electrical impulses. Rods and cones respond to different types of light input. Rods have high sensitivity to light. They can respond to a single photon, and their

response saturates at low light intensity. They are responsible for vision in dim light. Cones, on the other hand, are responsible for high acuity vision. They have low light sensitivity, which means that they respond only at high levels of light intensity. There are three types of cones, and each type responds maximally to light of different wavelengths, which enables color perception. The *fovea*, or central region of the visual field, contains only cones. This is the part of the visual field in which we have the greatest ability to perceive detail. Outside the fovea this ability drops off dramatically, which we generally do not notice, as we turn our head or eyes to focus the fovea on any detail we want to see. Rods outnumber cones 20 to 1 throughout the retina, but they are not present in the fovea.

After incoming light is transformed into electrical signals by the photoreceptors, it is transmitted from rods and cones through several cell types in the retina, which will not be discussed here. The final stage of retinal processing, before information is transmitted to the thalamus, is the retinal ganglion cells. Retinal ganglion cells have *center-surround receptive fields* (Kuffler 1952, Kuffler 1953), which provides the basis for downstream neural processing. This means that the ideal stimulus for a retinal ganglion cell is a bright spot on a dark background or a dark spot on a bright background at a given location in the visual field. It is important to note that in response to diffuse light, no response is evoked from retinal ganglion cells.

2.2.2 The Lateral Geniculate Nucleus

The lateral geniculate nucleus (LGN) is part of the thalamus, and links the retinal

ganglion cells to the visual cortex. Visual information is transmitted from the retina along the optic nerve, through the optic chiasm, to the LGN. At the optic chiasm, information from the left side of the visual field (from both the left and right eyes) crosses over to the right LGN, while information about the right visual field crosses over to the left LGN. Retinal cells project to the LGN such that there is a topographic map of the visual field in the LGN.

The LGN is organized in 6 layers, each of which receives a different type of input (Kandel et al. 2000). Each of the layers contains a complete retinotopic map, which means that every point on a given LGN layer maps to a corresponding point in the visual field. This mapping continues into the primary visual cortex.

LGN cells, like retinal ganglion cells, have center-surround receptive fields (Hubel and Wiesel 1961). Their responses are similar to those of retinal ganglion cells. These LGN cells provide input to cells in the visual cortex with more complex receptive fields.

The LGN takes in visual information from the retina and transmits it to the visual cortex, and receives feedback from the visual cortex as well (Hollander 1970, Kawamura et al. 1974, Updyke 1975) It also sends visual information elsewhere, for example, to the MT area (Rodman et al. 1989; Girare et al. 1992; Sincich, et al. 2004).

2.2.3 The Primary Visual Cortex

The primary visual cortex, V1, is the first level of cortical processing. It receives

feed-forward input from, and provides feedback to, the LGN. While some V1 cells have center-surround receptive fields like those in the LGN, this is the level of processing where cells first begin to respond to more complex stimuli (Hubel and Wiesel 1962).

Like the LGN, the primary visual cortex is arranged in 6 layers (Figure 2.4). The layers are numbered 1 through 6 according to their relative location in the cortex, with layer 1 closer to the cortical surface. Layers 2 and 3 are often referred to as layer 2/3 because they are virtually indistinguishable, while in primate layer 4 is subdivided into 4A, 4B, 4Cα and 4Cβ based on the origin of their inputs and the destination of their projections.

Input from the LGN is received primarily in layers 4Cα and 4Cβ (Hubel and Wiesel 1972, Le Vay and Gilbert 1977). Output to higher cortical areas is provided by layer 2/3 and layer 4B (Toyama et al. 1974, Gilbert and Kelly 1975), while layer 5 projects to the superior colliculus in the midbrain (Palmer and Rosenquist 1974) and layer 6 projects back to the LGN (Toyama et al. 1974, Hollander 1974, Gilbert and Kelly 1975).

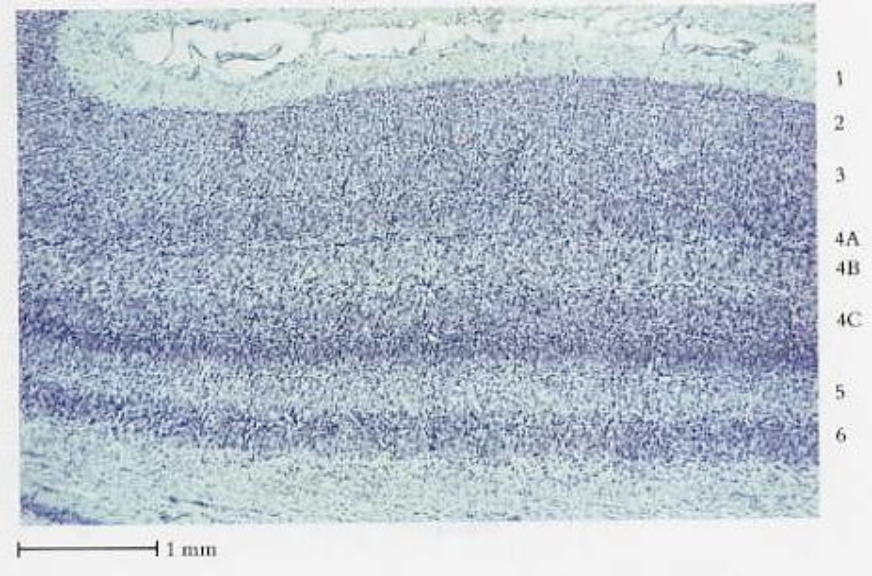

Figure 2.4 Laminar structure of the primary visual cortex (Hubel 1995).

Within V1, there are horizontal connections within each layer (McGuire et al 1991, Hirsch and Gilbert 1991, Bosking et al. 1997, Schmidt et al. 1997, Tamas et al. 1998) as well as vertical connections between layers (Fitzpatrick et al. 1985, Callaway and Wiser 1996, Stratford et al. 1996, Callaway 1998, McGuire et al. 1984, Ahmed et al. 1997). These connections create a circuitry that is partially responsible for different cell types found in V1. As one might expect, V1 cells that receive direct input from the LGN contain the simplest cell types, while cells that receive input from other V1 areas have more complex receptive field structures. Layer 4 contains both center-surround cells, like those found in the LGN, and simple cells (Gilbert 1977). Simple cells are the first level of visual processing following center-surround cells. Simple cells respond optimally to bars and edges (Hubel and Wiesel 1962). They typically prefer a bright bar on a dark background, a dark bar on a bright background, or a bright-dark edge. They are

orientation tuned, which means they respond maximally to a stimulus of a particular orientation. Simple cells are sensitive to the location of a stimulus within the receptive field, and will only respond to a bar or edge in the correct location.

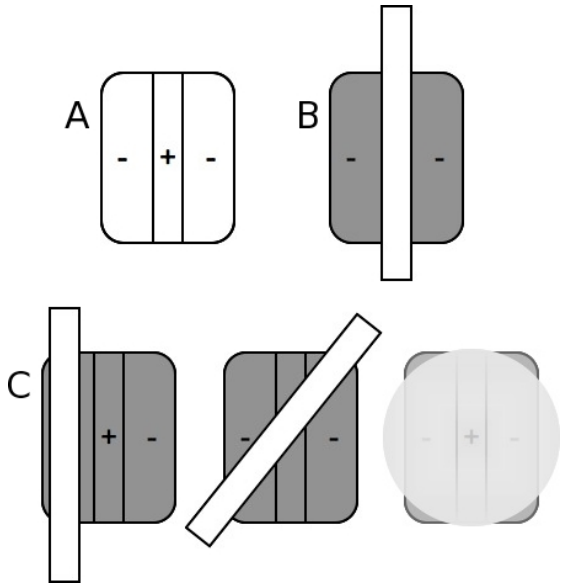

Figure 2.5 The simple cell receptive field. (A) A schematic of the receptive field of a simple cell that prefers a bright bar on a dark background. (B) The optimal stimulus for this cell. (C) Non-optimal stimuli: A bar in the wrong subfield, a bar of the wrong orientation, and diffuse illumination.

Most of the V1 cells outside of layer 4 are complex cells (Gilbert 1977). Complex cells receive input from simple cells. Like simple cells, they respond to oriented bars and edges, and are orientation tuned. However, they will respond to a stimulus of the preferred orientation regardless of location within the receptive field, and often respond to both bright and dark bars and edges. Within the category of complex cells there are important variations in receptive field properties. For example, complex cells in layer 6 have receptive fields that are longer and narrower than other complex cells, while layer

2/3 contains 20% end-stopped cells, which do not exist in any other layer (Hubel and Wiesel 1965).

Cells in the primary visual cortex are organized in orientation columns. This means that cells located in different layers of the cortex with the same position on the retinotopic map have the same orientation preference. Along the cortical surface, the orientation preference changes at a regular rate, rotating either clockwise or counterclockwise. The orientation preference of cells in the cortex has been mapped in many animals, including cat and macaque. An example from macaque using voltage sensitive dye is shown in Figure 2.6.

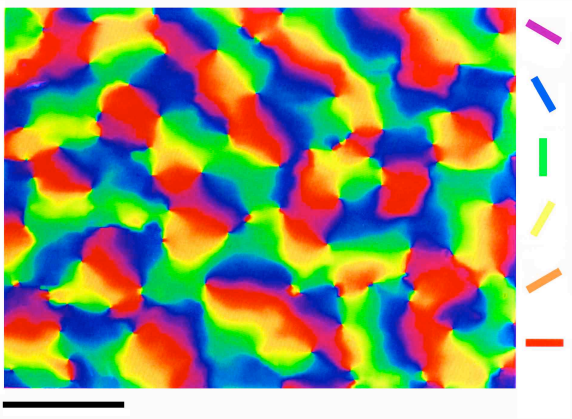

Figure 2.6 Orientation preference map in macaque. Scale bar = 1 mm. Adapted from Blasdel & Salama (1986).

2.2.4 The Extra-Striate Visual Cortex: V2, V4, IT

Following processing in V1, visual information is transmitted to various higher cortical areas. This thesis focuses mainly on early visual processing, so a brief explanation will suffice. The two stream hypothesis is often used to explain the

transmission of visual information through the cortex (Goodale and Milner 1992), and though it is still a controversial theory, it provides a basic way to look at the functions of the visual cortex. This hypothesis posits that information follows one of two streams. The dorsal ("where") stream is concerned with both motion and location in space. It originates in V1 and terminates in the parietal lobe, which integrates sensory information. The ventral stream goes from V1 to V2, V4, and IT, and is concerned with object recognition. Although this is an oversimplification of visual processing, it focuses on the two main functions of visual processing: determining what we see, and where it is located.

2.3 Experimental Background for Illusory Contour Detection

Computational modeling relies heavily on experimental work, both as a basis for developing theories and as a means of confirming theoretical predictions. An understanding of these techniques and results is vital to understanding the role that computational modeling can play in understanding cortical circuitry. The following is a brief description of experimental work in the field of illusory contour detection, including explanations of techniques used. Several key experiments will be highlighted.

An illusory contour is an image that is perceived as a contour in the absence of typical contour characteristics, such as a change in luminance or chromaticity across the stimulus. Illusory contours fall into two basic categories, abutting gratings and Kanizsa figures. The upper panel of Figure 2.7 shows two Kanizsa figures, and the lower panel shows two abutting gratings. The model described in this thesis deals exclusively with

abutting gratings, but experimental work on both types of stimuli has formed the basis for our understanding of illusory contour detection.

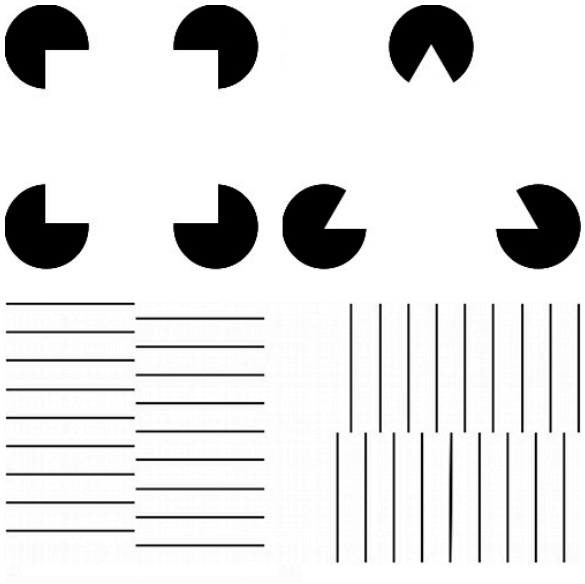

Figure 2.7 Two types of illusory contours. Kanizsa figures, which represent occlusion, shown are in the upper panel, and abutting grating contours are in the lower panel.

In cats and primates, cells that respond to illusory contours are sparse in cortical area V1, but are found in greater numbers in cortical area V2 (Von der Heydt and Peterhans, 1989, Sheth et al, 1996). *Single cell recording* and *optical imaging* are the primary experimental techniques that have been used to study illusory contour detection. These techniques have different applications, and different benefits. The following is a brief summary of the procedure and applications of these techniques in the field of illusory contour detection, including a representative sample of specific work using both techniques as applied to illusory contours.

2.3.1 Single Cell Recording

During single cell recording, an electrode is inserted into the brain of an animal through a small hole in the skull. It records the electrical activity at the precise location at which it is inserted, and can detect the action potentials of several neurons. Based on the properties of the measured signals, spike sorting can be used to extract the activity of a single neuron. During a recording session, the electrode is progressed through the section of the brain, and recordings are made at several adjacent locations. Although gross anatomy is known, it is not always possible to tell exactly which brain area the electrode is in. Therefore, in cases where the animal will be sacrificed, a current can be passed through the electrode at various points during the recordings to mark the location. When histology is performed later, it will be possible to tell where the recordings were made.

Single cell recording yields a great deal of information about single cell behavior. It is possible to measure with a great deal of accuracy (up to 1 ms) the timing of the neuron's response after a stimulus is presented (Bair 1999). It is also possible to detect subtle distinctions between cells in the same cortical area that would not be clear with optical imaging (see below).

The first, and perhaps most exhaustive, study of illusory contour detection was performed using single cell recording by Von der Heydt and Peterhans (1989). Figure 2.8 shows the results of a typical single cell recording, performed in an **awake, behaving** macaque (Von der Heydt and Peterhans, 1989). In A, a bright bar is moved through the receptive field of a V2 cell. Sixteen different orientations were used, as marked by the

white vertical bars on the left of the rastergram. (Two sample orientations are shown to the left of the plot.) At each orientation, the stimulus was moved back and forth through the cell's receptive field eight times. Each white point represents a single action potential. The neuron responds with the highest firing rate to a stimulus of the preferred orientation. In B, the same test is performed using an illusory contour. The cell's response is highest when the illusory contour is at the same orientation as in (A). The bottom panel of B confirms that the cell is not responding to the inducers by testing using a stimulus made up of the inducing lines without an illusory contour. This type of response indicates that the cell responds to both real and illusory contours.

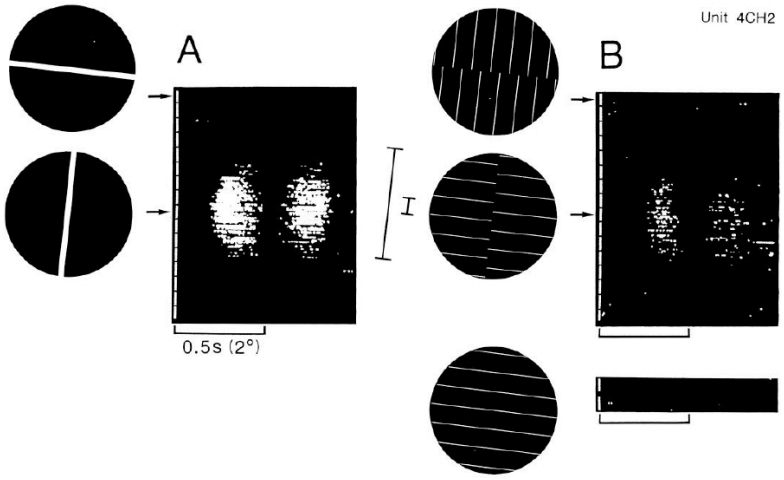

Figure 2.8 Single cell recording in primary visual cortex (V1) for real and illusory contours. The stimulus was moved back and forth through the receptive field of the neuron. Each white dot represents a single spike, and each row represents a different orientation (Von der Heydt and Peterhans, 1989).

Figure 2.9 shows orientation tuning of four V2 cells in response to real and

illusory contours. Tuning curves are a typical means of analyzing the orientation-dependent responses of neurons. The peak of the curve indicates the cell's preferred orientation, and the width shows how well tuned it is. This figure shows that the cells respond to both types of contours, but also underscores the variability across the responses. On the x-axis is the orientation of the stimulus, and on the y-axis is the firing rate of the neuron. In every case, the cells are tuned for both real and illusory contours. However, only C shows a cell that has similar response properties for both. In A, the cell responds more strongly to illusory contours than to real, and signals the orientation of the inducers as well. B shows a cell that responds to both types of stimuli, but responds much more strongly to real contours, and D shows a cell that responds to both real and illusory contours, but the responses are approximately 30 degrees apart in preferred orientation.

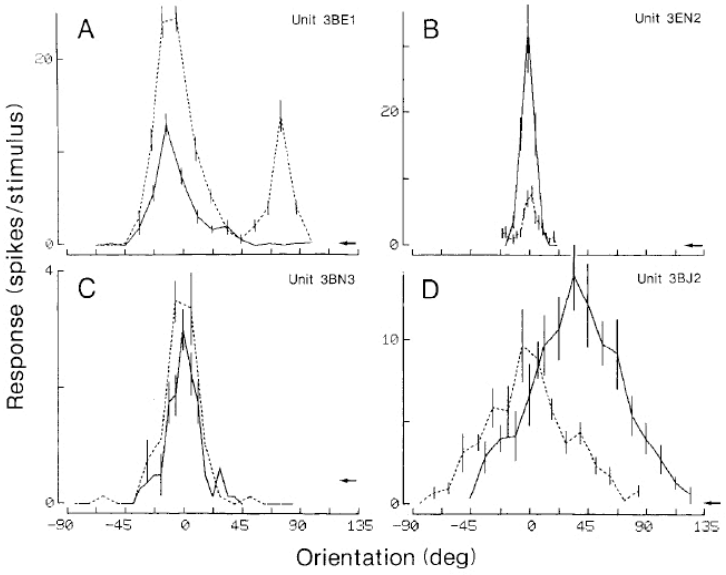

Figure 2.9 Orientation tuning curves from single cell recordings in macaque. Solid lines represent the response to real contours, and dashed lines represent the response to illusory contours. Adapted from Von der Heydt and Peterhans, 1989.

Several properties of V2 responses to illusory contours were measured by (Von der Heydt and Peterhans 1989), including the following: A) For most cells, the response to illusory contours is improved when the number of inducing lines is increased. Additionally, for some cells, there is a minimum threshold of inducing lines necessary to evoke a response to illusory contours, ranging from 2-8 inducing lines B) Cells can exhibit a variety of responses to changes in inducer line spacing. Some cells have a very specific preferred spacing (e.g. 0.2 degrees), and others respond similarly across a range of spacings. Currently, there is not enough data to fully characterize this property; however most cells recorded fall somewhere between these two extremes. C) When the orientation of the inducers is not orthogonal to the orientation of the illusory contours, there is often a shift in the peak of the tuning curve. Additionally, some cells do not

signal a contour at all if the inducers are slanted in a particular direction, while some respond to illusory contours independent of inducer slant.

The Von der Heydt and Peterhans study (1989) involved recordings from cells in areas V1 and V2. In V1, only 1 out of 60 cells tested was found to respond to illusory contours. In V2, however, 45 out of 103 V2 cells showed an illusory contour response. Based on this, one of the conclusions of this study was that cells in V2 respond to illusory contours, while cells in V1 do not.

Peterhans and Von der Heydt (1989) proposed a particular circuitry for the detection of illusory contours based on these recordings, represented by the diagram in Figure 2.10. They suggested that cells that detect illusory contours receive input both from complex cells with parallel orientation preferences and end-stopped cells with orthogonal orientation preferences. This circuitry has not yet been confirmed experimentally, but it is a widely accepted theory for the circuitry behind illusory contour detection and is the basis of my model.

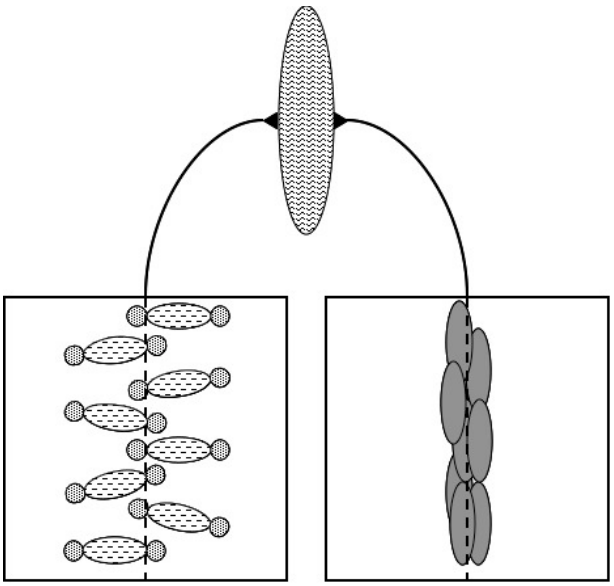

Figure 2.10 Proposed wiring scheme for cells that can detect illusory contours. The upper cell is a complex V2 cell capable of responding to illusory contours. The cells in the left panel are end-stopped cells, and the cells in the right panel are complex cells.

2.3.2 Optical Imaging

In order to make use of as much information as possible, different experimental techniques are used to examine different aspects of the same problem. As discussed previously, single cell recordings provide a great deal of information about neuronal dynamics. However, although a set of single cell recordings can contain data from hundreds of neurons, there are millions of neurons in the visual cortex alone so reasonable inferences about population dynamics cannot be made based on single cell recordings alone. For this kind of information, we use optical imaging. During optical imaging, a portion of the skull is removed, and a clear surface covering is installed in its place. Via this window, the activity of a portion of the brain can be monitored based on the presence of oxygen. Hemoglobin is the protein that carries oxygen in blood, and

oxyhemoglobin (hemoglobin bound with oxygen) and deoxyhemoglobin (hemoglobin without oxygen) have different absorption spectra. When a section of the brain is active, more oxygen is needed, and the relative presence of oxy- and deoxyhemoglobin indicate how much activity is occurring in a brain area. The results of optical imaging are a series of digital images, in which each pixel represents a group of adjacent neurons.

Optical imaging has certain limitations. It is only possible to use the surface of the brain closest to the skull, and does not allow recording from within the sulci, or from deep brain areas. It is limited by time resolution – the time scale for intrinsic imaging is on the order of seconds, while the precision of neural activity is on the order of ms (Bair 1999, McCormick, Connors and Lighthall 1985). It also does not allow for very precise spatial resolution, either—a single pixel does not represent a single cell. It does, however, have one distinct advantage—it allows us to make inferences about populations of neurons (which is not possible with single cell recording) and thereby predict perceptual outcomes. Optical imaging is important from this perspective because it gives us a clear way to look at entire neural populations.

It is important to remember, however, that neither the results of single cell recording nor of optimal imaging should be interpreted as equivalent to perception. As an example, see the results of (Ramsden and Roe 2001) described below. In this case, optical imaging shows population results in V1 that appear to be the opposite of perception. (Figure 2.14)

Several studies, in both cat and primate, have used optical imaging to analyze V1 and V2 responses to illusory contours. Figure 2.11 shows predicted results of an optical

imaging study, depending on whether or not the area imaged responds to illusory contours (Sheth et al 1996). During optical imaging, areas that respond to the stimulus show the highest activation, while the areas that do not respond show the lowest activation.

Figure 2.11 shows the results of a hypothetical optical imaging experiment, depending on whether or not a given area of the cortex responds to illusory contours. In A, the green areas represent the section of the cortex that is the most highly activated by vertical real contours. If this part of the brain responds to both real and illusory stimuli, then the neurons in the green areas would also be the most highly activated ones for vertical illusory contours. However, if this part of the brain does not respond to illusory contours, then the response will look like the right panel—vertical illusory contours will cause activation in the red areas, which are the areas activated by horizontal real contours. (This would imply that these areas only respond to the inducing lines in the stimulus). B shows a histogram of responses in these two cases. Each pixel in the image will show maximum activation for a given orientation of real contours, and for a given orientation for illusory contours. B shows the distribution of the differences in these two cases—if the area studied responds to illusory contours, the difference in preferred orientation of the majority of the pixels will be close to zero. On the other hand, if the area studied does not respond to illusory contours, the difference in preferred orientation between the two cases will be 90 degrees.

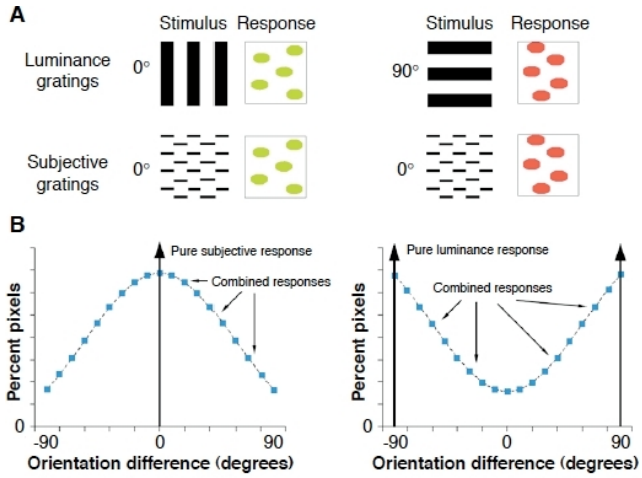

Figure 2.11 Predicted results of optical imaging. Predictions for cells that respond to both real and illusory contours are shown on the left, while cells that respond only to real contours are shown on the right (Adapted from Sheth et al. 1996).

Figure 2.12 shows optical imaging results in cat area V2/A18. Panel A shows the response to a single real contour, and B shows the response to a single illusory contour. The dark areas are the areas of highest activation, while the bright areas are the areas of lowest activation. These maps were taken for a range of orientations, and the preferred orientation for each pixel was determined. The maps of preferred orientations are shown for real (C) and illusory (D) contours. Each pixel in C and D is color-coded based on the orientation that evoked the highest activation of that pixel. Panel E shows a map of the differences between C and D, and F shows a histogram of the points in E. These results indicate that cat area V2/A18 does respond to illusory contours, as the majority of the cells are maximally activated by the same orientation of real and illusory contours.

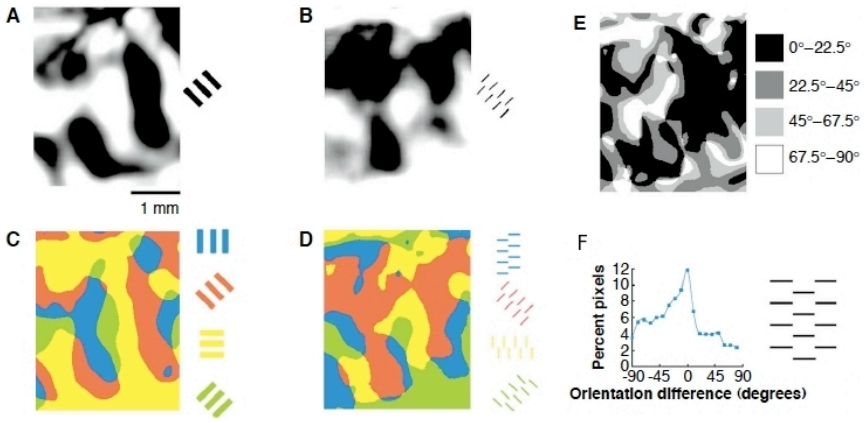

Figure 2.12 Optical imaging results in cat area A18. Adapted from Sheth et al, 1996. A) Optical imaging response for a real contour stimulus with a 135-degree orientation. Black indicates the most highly activated area. B) Optical imaging response for an illusory contour stimulus with a 135-degree orientation. C) Orientation preference map developed based on real contour responses. D) Orientation preference map developed based on illusory contour responses. E) Map of the difference in orientation preference for real and illusory contours. F) Histogram of the values in E.

Figure 2.13 shows the results of the same test performed in area V1/A17. These results look more similar to the right panel in Figure 2.11, indicating that cells in area 17 respond primarily to the inducing lines. However, a percentage of the neurons did respond more strongly to the orientation of illusory contours than to the orientation of real contours. Based on this, the study concluded (contrary to previous single-cell studies in macaque) that illusory contour responses are seen in V1 as well as V2, albeit to a lesser extent.

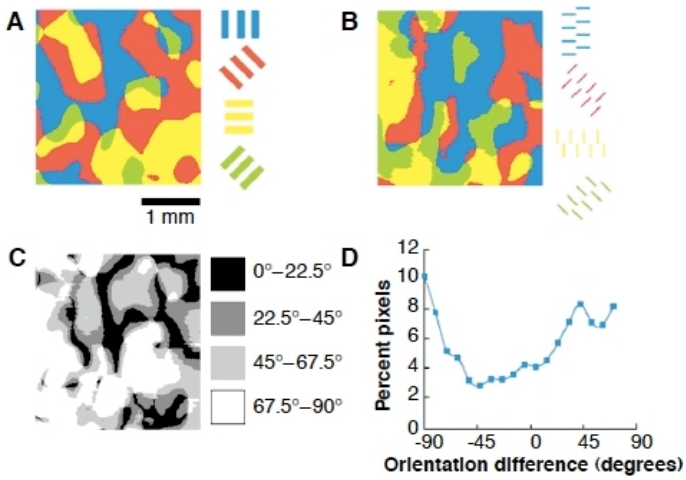

Figure 2.13 Optical imaging results in cat area A17. Adapted from Sheth et al, 1996. A) Orientation preference map developed based on real contour responses. B) Orientation preference map developed based on illusory contour responses. C) Map of the difference in orientation preference for real and illusory contours. D) Histogram of the values in C.

Figure 2.14 shows the result of another optical imaging experiment in V2 (Ramsden et al. 2001), performed in anesthetized primate. In this experiment, optical imaging was done using a pair of stimuli with orthogonal orientations and the difference between the resulting images is displayed. The images shown reflect the modulation of the response between to sets of stimuli. In B, the black areas are more highly activated by horizontal stimuli and are circled in orange, while the white areas are more highly activated by vertical stimuli and are circled in blue. In C, the same test is performed using illusory stimuli. As in B, the black areas are more highly activated for horizontal illusory contours, while the white areas are more highly activated for vertical illusory contours. Note that the inducers are the same orientation in both cases, so any response to the orientation of the inducing lines is subtracted out. Because the orange and blue circles from B overlay black and white areas, respectively, in C, area V2 appears to have

the same response modulation for real and illusory contours.

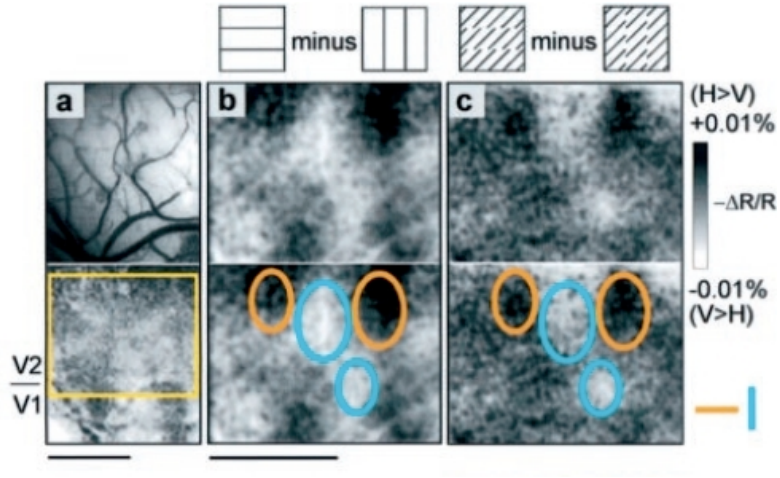

Figure 2.14 Optical imaging in anaesthetized primate area V2. Adapted from Ramden et al., 2001. A) Blood vessel landmarks (top) and ocular dominance map (bottom). The yellow box indicates the area shown in (B) and (C). B) Difference between the optical imaging response to horizontal and vertical real contours. Dark areas indicate strongest response to horizontal, light areas indicate strongest response to vertical. The lower panel shows the areas that respond most strongly to horizontal circled in orange, and the areas the respond most strongly to vertical circled in blue. C) Difference between the optical imaging response to horizontal and vertical illusory contours. Dark areas indicate strongest response to horizontal, light areas indicate strongest response to vertical. The lower panel shows the same orange and blue circles from (B): The same areas that respond to horizontal real contours also respond to horizontal illusory contours, and the same areas that respond to vertical real contours also respond to vertical illusory contours.

Figure 2.15 shows the same experiment performed in V1. Panel A shows the modulation of the real response, where areas that are most active in response to horizontal are real and are circled in orange, while the areas that are most active in response to vertical are white and are circled in blue. B shows the modulation of the

illusory response, where areas that prefer horizontal are black and areas that prefer vertical are white. However, in this case, the activation is reversed, which can be seen by the placement of the orange and blue circles. Areas that are most activated by horizontal real contours (orange circles) are most activated by vertical illusory contours, and vice versa. The inducing lines for all illusory stimuli are the same orientation (at a 45 degree angle to the illusory contour) so any response to the inducing lines is subtracted out. The authors present the hypothesis that this surprising result is likely due to inhibitory feedback to V1 from higher cortical areas.

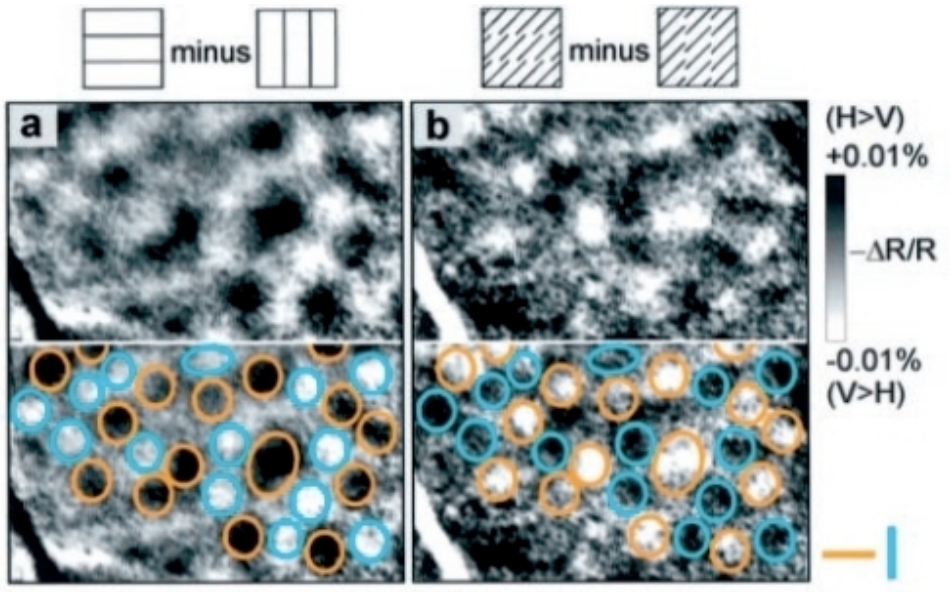

Figure 2.15 Optical imaging in anaesthetized primate area V1. Adapted from Ramden et al. (2001). A) Difference between the optical imaging response to horizontal and vertical real contours. Dark areas indicate strongest response to horizontal, light areas indicate strongest response to vertical. The lower panel shows the areas that respond most strongly to horizontal circled in orange, and the areas the respond most strongly to vertical circled in blue. B) Difference between the optical imaging response to horizontal and vertical illusory contours. Dark areas indicate strongest response to horizontal, light areas indicate strongest response to vertical. The lower panel shows the same orange and blue circles from (A): The same areas that respond most strongly to horizontal real contours respond most strongly to vertical illusory contours, and vice versa.

The idea that activation in V1 could be due to feedback from higher levels is supported by experiments done by Lee and Nguyen (2001). Using single cell recordings and Kanizsa figure illusory contours, they found that the onset of illusory contour response in V1 is 30 msec later than in V2. Their studies support the hypothesis that V1 responses to illusory contours is due to feedback from higher cortical areas.

2.4 Computational Background

To date, several types of models for illusory detection have been proposed. They have been able to explain certain aspects of illusory contour detection, but still leave many questions unanswered. These models have provided the foundation for my work, which seeks to build on what we already know and further explore the mechanism behind illusory contour detection. In order to illustrate the present state of the field and provide context for explaining the novel characteristics of my model, the following is a brief summary of some of the computational work that has preceded mine.

One of the most basic models is the filter-rectify-filter model proposed by (Zhan and Baker 2008). In this case, an illusory contour stimulus is first integrated over a filter representing early processing. The result is rectified using a sum of squares, and filtered again using a filter representing an illusory contour detecting cell. The result then shows correct orientation tuning for illusory contour stimuli. The filter is represented by the equations $R_s(f) = e^{-\frac{[\log_2(f)\log_2(f_p)]^2}{2\sigma_f}}$ and $R_O(\theta) = e^{-\frac{(\theta-\theta_p)^2}{2\sigma_O^2}}$, where R_S and R_O are the filters for spatial frequency and orientation, respectively. R_S uses different parameters for the A17 and A18 cells, and R_O is used at a variety of preferred orientations. The representations of the filters in Fourier space (at all orientations) are shown in A and B of Figure 2.16. Panel A shows the receptive fields of A17 cells, which are sensitive to stimuli with higher spatial frequencies, up to 1.92 cycles per degree (cpd) while B shows the receptive fields of A18 cells, which respond to lower spatial frequencies, up to 0.48 cpd. Panels C and D show two of the illusory contour stimuli used in the model (left panels) and their representation in Fourier space (right panels). Superimposed on the right panels is the

area that contains the receptive fields of A18 cells. These receptive fields do not overlap with the illusory contour stimuli in Fourier space, so their response to these stimuli would be zero. G and H show the same stimuli after A17 filtering and rectification. Their Fourier representation is shown in the right panel. After filtering and rectifying, the stimuli are filtered by the A18 cells, which now are able to respond to illusory contours.

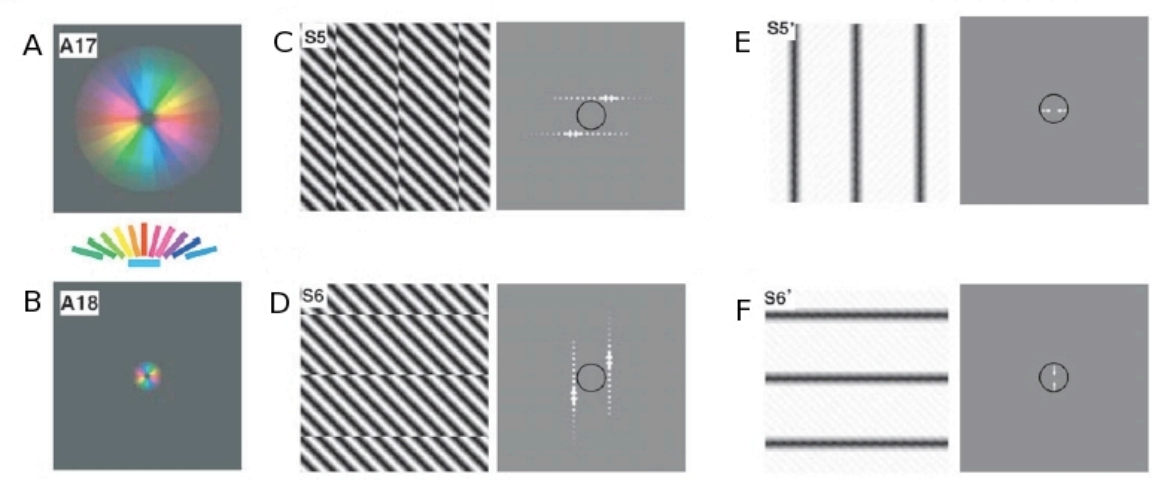

Figure 2.16 Results from a computational model. Adapted from Zhan and Baker (2008). A) Receptive field of model V1 cells in Fourier space. B) Receptive fields of model V2 cells in Fourier space. C, D) Illusory contour stimuli (left) and their representation in Fourier space (right). They fall outside the receptive fields of V2 cells. E,F) The same stimuli, after being filtered by V1 cells (left), and their new representation in Fourier space (right). After V1 filtering, they fall within the receptive fields of V2 cells.

The first stage of many contour-detecting models is a Gabor filter, as described above. This has been shown to accurately model the behavior of simple cells (Jones and Palmer 1987). It is the basis of a model by (Heitger et al. 1998), who created a model for illusory contour detection by building up responses for complex cells and end-stopped

cells beginning with simple cells modeled as gabors, and grouped these responses to achieve detection of illusory contours. This technique provided the basis for my work. Their model was able to show population responses that could reconstruct both types of illusory contours, as shown in Figure 2.17. Panels A and B show examples of the types of stimuli presented to the model, and C and D show the response their model would give to these stimuli. However, a model of this type is not able to reproduce the types of single-cell responses measured by (Von der Heydt and Peterhans 1989).

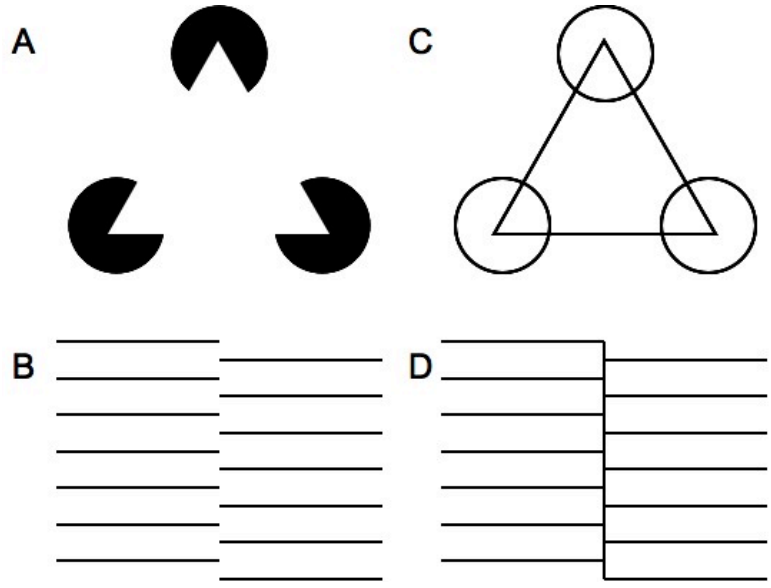

Figure 2.17 Results of a model for illusory contour detection (Heitger et al. 1998) A and B show examples of two types of stimuli this model is able to respond to. C and D show the line segments perceived by this model for stimuli A and B.

2.5 Modeling Topographic Organization of Neurons: Self-Organizing Maps

A self-organizing map is a means of reducing data of multiple dimensions into one or two dimensions. It uses unsupervised learning to map a set of values onto a matrix in a way that preserves the relative distances between data points. This technique employs neighborhood function that has a smoothing effect, resulting in a map consisting of clusters of similar values (Kohonen 1995).

This technique has been shown to accurately reproduce the orientation preference maps found in the visual cortex (Kohonen 1982). In this case, the orientation preference of cells is mapped over the x-y spatial location of the neurons in a way that accurately corresponds to maps measured experimentally. This has been used previously to represent orientation preference maps in computational models of the visual cortex, but never before in the context of illusory contour detection.

2.6 Simulating Supervised Learning: Support Vector Machines

A support vector machine (SVM) is a supervised learning technique used to divide a set of data based on a particular characteristic (Boser, Guyon and Vapnik 1992; Cortes and Vapnik 1995). The SVM is trained on a set of data for which the classifications are known (the training set), and is then tested on a second set (the test set), and its performance is measured based on how well it correctly classifies the test data.

SVM is an approach that can be used to solve classification problems in many

fields, from speech recognition to protein folding. In this case, we are using it to model figure-ground separation in the visual cortex. We present the model with similar, but varying stimuli, and use an SVM to distinguish when a particular component of the stimulus is in the foreground or the background.

The following is a brief explanation of the fundamentals of SVMs. This explanation is based on the work by (Burgess, 1998), and more information can be found by referencing this work.

We assume a set of data in n dimensions. Each point is defined by a vector $\mathbf{x}_i$, and has an associated label y_i. We want to divide the data based on the values of y_i. In order to do this, we divide the space $\mathbf{R}^n$ using an oriented hyperplane.

2.6.1 The Linear, Separable Case

We begin by considering the simplest possible arrangement, a set of *m* data points that has two possible values for y_i, -1 and 1, and is linearly separable. We define a hyperplane that divides the data set, such that **w** is the vector that is perpendicular to the hyperplane, and b is the distance from the hyperplane to the origin (Figure 2.18). The optimal hyperplane is such that the distance from it to the nearest data points on either side is maximized. Let d_+ and d_- be the distances to the nearest positive and negative data points, respectively. The sum of these two distances (d_++d_-) is called the margin, indicated in the figure by the marginal hyperplanes H_1 and H_2. These nearest data points that lie on the hyperplanes H_1 and H_2 are called support vectors. They are crucial in

determining the solution, and their removal would change the solution of the problem. An optimal hyperplane has the largest possible margin.

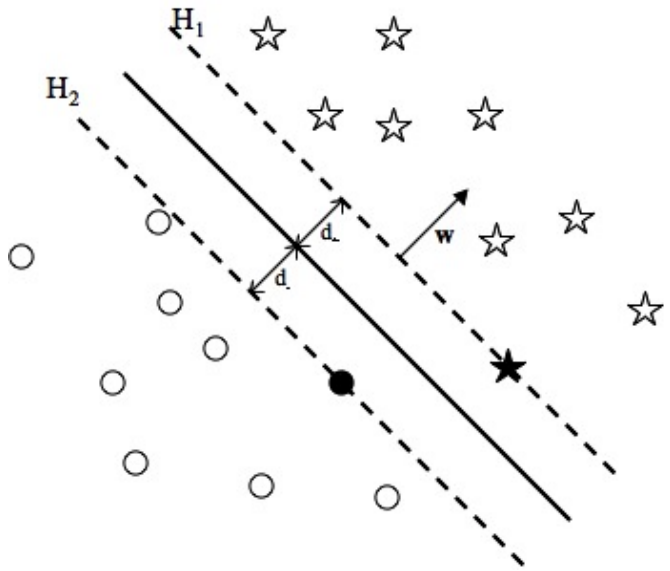

Figure 2.18 A linearly separable data set. Circles and stars are the two data sets. The support vectors are represented by filled in symbols.

We assume that the data set satisfies the following constraints,

$$\begin{cases} \mathbf{x}_i \cdot \mathbf{w} + b \geq +1, & for\ y_i = +1 \\ \mathbf{x}_i \cdot \mathbf{w} + b \leq -1, & for\ y_i = -1 \end{cases}$$

They can be rewritten as one set of inequalities as follows:

$$y_i(\mathbf{x}_i \cdot \mathbf{w} + b) - 1 \geq 0, \quad i = 1,...,m$$

Training the support vector machine amounts to minimizing the Lagrangian:

$$L_P \equiv \frac{1}{2}\|\mathbf{w}\|^2 - \sum_{i=1}^{l} \alpha_i y_i (\mathbf{x}_i \cdot \mathbf{w} + b) + \sum_{i=1}^{l} \alpha_i$$

under the constraints that the derivative with respect to all the α_i is zero and all $\alpha_i>0$, where α_i are the Lagrange multipliers. This results in the equations:

$$\begin{cases} \mathbf{w} = \sum_i \alpha_i y_i \mathbf{x}_i \\ \sum_i \alpha_i y_i = 0 \end{cases}$$

Note that there is a Lagrange multiplier for every training point. The points for which $\alpha_i>0$ are the support vectors, and lie on the hyperplanes H_1 and H_2. All other points have $\alpha_i=0$. This means that the support vectors are the critical elements of the training set: removing any of the other points, or moving them in any way that does not involve crossing the marginal hyperplane, would not alter the solution. Since the objective function is convex, and the points satisfying the constraints form a convex set, this is equivalent to maximizing L_p under the constraints that the gradients of L_P with respect to **w** and b are zero and all $\alpha_i \geq 0$. This should occur at the same values of **w**, b and α as the minimization problem.

We can recast the problem as an optimization problem. In this case, the Karush-Kuhn-Tucker (KKT) constraints are necessary and sufficient for **w**, *b*, α to be a solution, if the problem is convex and regularity conditions hold (Fletcher 1987). Finding a solution to the KKT constraints is equivalent to solving the SVM problem. For our problem, the conditions are (Fletcher 1987):

$$\begin{cases} \dfrac{\partial}{\partial w_\nu} L_P = w_\nu - \sum_i \alpha_i y_i x_{i\nu} = 0 \quad \nu = 1,...,n \\ \dfrac{\partial}{\partial b} L_P = -\sum_i \alpha_i y_i = 0 \\ y_i(\mathbf{x}_i \cdot \mathbf{w} + b) - 1 \geq 0 \quad i = 1,...,m \\ \alpha_i \geq 0 \quad i = 1,...,m \\ \alpha_i(y_i(\mathbf{x}_i \cdot \mathbf{w} + b) - 1) = 0 \quad i = 1,...,m \end{cases}$$

2.6.2 The Linear, Non-Separable Case

If a data set is non-separable, we can still use SVMs for classification. To solve this problem, we relax the constraints, adding the variable ξ_i such that for points on the wrong side of the marginal hyperplane, $\xi > 0$, and for misclassified points, $\xi > 1$ (Figure 2.19). This will be accompanied by a penalty, that is, an increase in the objective function for each point on the wrong side of the marginal hyperplane or misclassified. The Lagrangian then becomes

$$L_P = \frac{1}{2}\|\mathbf{w}\|^2 + C\sum_i \xi_i - \sum_i \alpha_i \{y_i(\mathbf{x}_i \cdot \mathbf{w} + b) - 1 + \xi_i\} + \sum_i \mu_i \xi_i$$

where C is a parameter chosen by the user that gives the magnitude of the penalty, and μ_i are Lagrange multipliers used to ensure that ξ_i are positive. As before, the solution can be found using the KKT conditions.

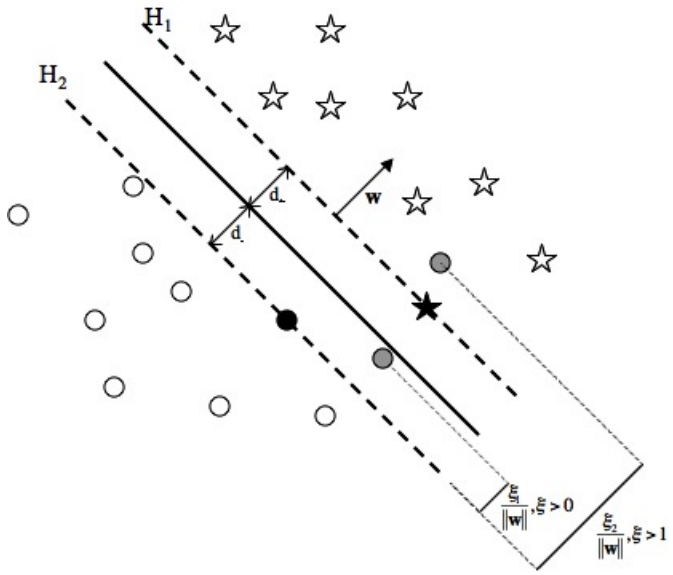

Figure 2.19 A data set that is not linearly separable. Support vectors are shaded black and gray, where gray indicates vectors that are misclassified.

2.6.3 The Non-Linear Case

The majority of data sets cannot be separated by a linear function. In such cases, we are able to map the data into a space in which it can be solved by a linear function, using a mapping function Φ (Boser, Guyon and Vapnik 1982). Because the SVM depends on the dot products of the $\mathbf{x_i}$, and not on the individual vectors, we can simplify the problem by using function that defines the dot product $\mathbf{x}_i \cdot \mathbf{x}_j$ in the new space. We look for a kernel function K such that $K(\mathbf{x}_i, \mathbf{x}_j) = \Phi(\mathbf{x}_i) \cdot \Phi(\mathbf{x}_j)$. Then, in order to project our data into Φ-space, we replace $\mathbf{x}_i \cdot \mathbf{x}_j$ with $K(\mathbf{x}_i, \mathbf{x}_j)$. This allows us to work in the new space without having to work with (or know) the function Φ.

There are many possibilities for kernels, and the choice depends on the characteristics of the data set. The most commonly used one is the Gaussian kernel:

$$K(\mathbf{x}_i, \mathbf{x}_j) = e^{-\frac{\|\mathbf{x}_i - \mathbf{x}_j\|^2}{2\sigma^2}}$$

This is also the kernel we use in our model.

Finally, we want to point out that although we decided to have binary classifiers, they can easily be combined to solve multiple-classification problems.

Chapter III

A neural model of the visual cortex: detection of real and illusory contours

3.1 Introduction

One of the fundamental tasks that our brain performs as part of visual processing is the detection of contours. This can be a very complex task, as contours are not always clearly defined: for example, the central stimulus represented in Figure 3.1 is perceived as a vertical line through the center of the image despite the fact that no such line exists; instead the perception of a line is induced by appropriately aligned horizontal bars (illusory contour). Within the cortex, the processing of visual information takes place in several stages, beginning with the primary visual cortex (area V1) and continuing through areas V2, V4 and the inferotemporal cortex (IT) (Felleman and Van Essen 1991). Each stage corresponds to a new level of complexity: neurons in area V1 are selective for the orientation of bars and edges (Hubel and Wiesel 1965), while neurons in IT display selectivity for intricate shapes and forms (Gross et al. 1972). Experimentally, neurons that respond to illusory contours have been found in cortical areas of the rhesus monkey (Von der Heydt and Peterhans 1984; Von der Heydt and Peterhans 1989; Lee and

Nguyen 2001) and cat (Sheth et al. 1996, Zhan and Baker 2008).While cells that are tuned to the orientation of the illusory contours rather than the inducing lines have been found in several visual areas including V1, V2 and IT, there is an increasing consensus that the first cells to detect illusory contours are located in area V2 (Von der Heydt et al 1984, Von der Heydt and Peterhans 1989, Sheth et al 1996, Lee and Nguyen 2001, Pillow and Rubin 2002). Furthermore, the latencies of the responses of these cells suggest that they respond to the orientation of the illusory contours before receiving feedback from higher cortical areas such as V4 and IT (Lee and Nguyen, 2001).

To date, several models have been proposed to explain illusory contour detection (Heitger et al. 1992; Heitger and von der Heydt 1993; Finkel and Edelman 1989; Grossberg and Mingolla 1985; Peterhans et al. 1986; Skrzypek and Ringer 1992; Ullman 1976). However, these models do not take into account the topographic organization of V1 neurons. Experimental evidence indicates that orientation preference is mapped non-homogeneously throughout V1, hence not all orientations are equally present at all locations (Hubel and Wiesel 1974; Ts'o et al. 1990; Blasdel and Salama 1986). (For comparison, the area of a typical V2 cell receptive field in cat is between 2 and 8 degrees^2 (Hubel and Wiesel 1965), while the area of a V1 cell typically ranges from 0.2 to 8 degrees^2 (Hubel and Wiesel 1962).) It is not clear whether these models are still able to respond to illusory contours when a realistic topographic organization is taken into account. Furthermore, the behavior of individual model cells is not accessible using these models. Experimentally, V2 cells display a variety of properties such as orientation tuning for real and illusory contours and inducer spacing preference (Von der Heydt and Peterhans 1989). The question of whether these properties are consistent with the

proposed mechanisms of illusory contour detection has not been adequately addressed by previous models (Heitger et al. 1992; Heitger and von der Heydt 1993; Grossberg and Mingolla 1985; Peterhans et al. 1986; Skrzypek and Ringer 1992; Ullman 1976).

We propose a model that incorporates realistic orientation preference maps at the level of V1. This model is based on principles outlined in (Von der Heydt and Peterhans, 1989) and includes V2 cells that are able to respond to both illusory and real contours.

3.2 Model overview

Experimental evidence indicates that detection of illusory contours can be accomplished as early as V2 (Von der Heydt and Peterhans, 1989, Sheth et al., 1996, Lee and Nguyen, 2001). We suggest that for this detection only feed-forward input is necessary from cells found in areas V1 and V2 of the visual cortex. The first stage of our model consists of four computational stages, representing four cell types known to exist in these cortical areas. Specifically, these types are (1) simple cells, (2) complex cells, (3) end-stopped cells, and (4) illusory-contour-detecting cells, henceforth referred to as pattern cells. The second stage of our model consists of classifier units, which model the behavior of cell types in the inferotemporal cortex (IT). A schematic of the model is shown in Figure 3.1. The simple, complex and end-stopped cells in the model correspond to cell types in area V1, while the pattern cells in the model correspond to the V2 cells that respond to illusory contours. The topographical arrangement of V1 cells in the model is characterized by a non-homogeneous orientation map generated so as to correspond to

those observed experimentally (Hubel et al. 1978; Blasdel et al. 1986; Grinvald et al. 1986). The same orientation map is used for each V1 cell type, and is modeled using the techniques described in (Kohonen 1982). Each neuron is characterized by a unique set of (x,y,θ) coordinates, where (x,y) is the retinotopic position and θ is the cell's preferred orientation. There are 16 possible preferred orientations for the model neurons, spanning the range $[0°, 180°]$. The orientations are evenly distributed across the model cortex. For V2 cells, all orientations are uniformly distributed across the visual field.

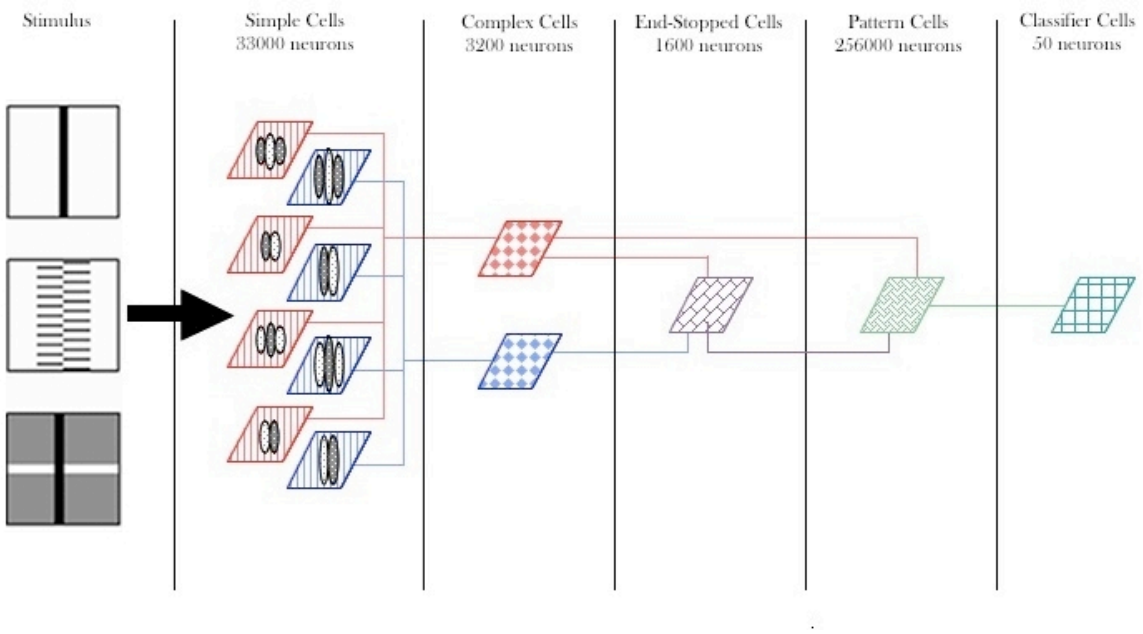

Figure 3.1 Schematic of the model. The model consists of five levels of processing. Each level contains a different cell type. The first three levels contain cell types corresponding to cells in the primary visual cortex (V1). The fourth level contains cells that respond to illusory contours, belonging to V2. The fifth level contains cells capable of performing simple figure-ground segregation tasks.

We assume a network as described in (Dayan and Abbott, 2001). For simplicity, we make the following assumptions: a) a time-independent firing rate such that the

synaptic input current to pattern cells follows the form $I_S = \vec{w} \cdot \vec{u}$ (where I_s is the synaptic current, *w* are the synaptic weights, and *u* are the firing rates of presynaptic cells) and b) an activation function given by a threshold linear function $F(I_s) = \left[I_s - \gamma \right]_+$ (where γ is the threshold).

3.2.1 Stimulus Generation

The model was presented with light and dark stimuli spanning 8x8 degrees of visual field. The stimuli were generated using square waves, and consisted of a matrix comprised of values between -1 and 1, with negative values corresponding to dark pixels and positive values corresponding to bright pixels. The positive or negative values were arranged in bar shapes on a background of zero (Figure 3.1, Stimulus).

A real contour stimulus was a bar of width 0.4 degrees (the width of a simple cell subfield) and, unless otherwise stated, a length spanning the full extent of the visual field. Illusory contours were abutting gratings comprised of inducers that were 1.2 degrees long, 0.1 degrees wide, and 0.7 degrees apart. Crossed-bar stimuli, used in the figure-ground segregation task, consisted of two bars, each full-field in length and 0.4 degrees in width.

3.2.2 Simple Cells

The first stage of the model consists of excitatory and inhibitory simple cells.

This stage contains eight groups of cells, each with a different set of receptive field properties. These cells are modeled after simple cells found in V1, and, like simple cells, they respond to oriented bars and edges. A Gabor function (Eq. 1) has been shown to accurately represent the receptive field of simple cells (Jones and Palmer 1987).

$$RF = e^{-\frac{(x-x')^2}{2\sigma_x^2}} e^{-\frac{(y-y')^2}{2\sigma_y^2}} \cos(kx + \varphi) \qquad (1)$$

Equation 1 describes the receptive field of a neuron whose center is at the position (x',y'), using coordinates (x, y) that are rotated according to the cell's orientation preference. The variable φ defines the spatial phase of the neuron, and determines the subfields of the receptive field. These subfields designate which areas of the receptive field respond to light (ON) and dark (OFF). Experimentally, although φ can take a continuum of values in the interval [0, 2π], values that are multiples of π/2 are predominant (Field and Tollhurst 1986, Ringach 2002). In this model, there are four possible values for φ: 0, π/2, π, 3π/2, which correspond to cells with OFF-ON-OFF, ON-OFF, ON-OFF-ON or OFF-ON subfields respectively (depicted in the simple cell area on the schematic of the model in Figure 1). Each type of receptive field comes in two sizes, resulting in a total of eight groups of cells. Each group of simple cells is represented in the model by a 64x64 matrix, with orientation preferences defined by the non-homogeneous orientation map described above. There are four groups of simple cells with small receptive fields that provide input to excitatory complex cells, and four groups

of simple cells with large receptive fields that provide input to inhibitory complex cells. Their parameters are summarized in Table 1.

	Small RF	Large RF
σ_x (deg)	0.25	0.40
σ_y (deg)	0.50	0.80
k	8	5
ϕ	0, π/2, π, 3π/2	

Table 1. Simple Cell Receptive Field Sizes

These parameters yield simple cells with subfield widths of 0.4 and 0.6 deg and lengths of 2.2 and 3.4 deg respectively, in good agreement with experimentally observed values (Palmer 1981, Heggelund 1986, Pei 1994)

The firing rate of a simple cell is obtained by the integration of the Gabor function representing the receptive field (Eq. 1) with the stimulus S(x,y):

$$R_S = [\iint S(x-x', y-y') \cdot RF(x', y')\, dx'\, dy' + R_{S,bl}]_+ \qquad \textbf{(2)}$$

where $R_{S,bl}$ is the baseline firing rate of simple cells and is equal to 5 Hz (Ringach et al. 2002), and the notation $[]_+$ indicates positive rectification. The stimulus that yields the highest simple cell response consists of bright bars in the on-subfields and dark bars in the off-subfields. Because simple cells typically have two or three subfields, this corresponds to a bright bar on a dark background, a dark bar on a bright background, or a bright-dark edge.

This stage of the model contains 32,768 simple cells (8 x 64 x 64).

3.2.3 Complex Cells

Complex cells are a cell type found in areas V1 and V2 that, like simple cells, are orientation tuned. Experimentally, complex cells display a variety of properties. For the purposes of this model, we assume two properties that have been widely observed: position invariance and phase invariance. This means that, unlike simple cells, complex cells respond to a bar or edge of the correct orientation regardless of its location in the cell's receptive field, and regardless of whether it is dark or bright. Spatial and phase invariant responses of complex cells have been previously modeled both through feed-forward and recurrent mechanisms. Feed-forward models either linearly sum inputs from several simple cells of similar orientation and spatial frequency preferences but different phases (Hubel and Wiesel 1962) or sum the squared inputs from four simple cells with same orientation and spatial frequency preferences but phases that increase in increments of $\pi/2$ (Pollen and Ronner 1982). Recurrent models assume that spatial and phase invariance is the result of recurrent connections between complex cells that receive input

from a relatively narrow range of spatial phase preferences. (Chance et al, 1999). In our model the complex cell firing rate is modeled according to the energy model of (Pollen and Ronner 1982). Each complex cell in the model receives input from four concentric simple cells, one of each phase. The location of the receptive field center and preferred orientation of these cells matches that of the complex cell to which they provide input. The firing rate of complex cells in the model is

$$R_C = \sqrt{\sum w_{odd} R_{S,odd}^2 + \sum w_{even} R_{S,even}^2} \quad , \qquad \textbf{(3)}$$

where odd and even refer to whether the simple cell's RF has two or three subfields, respectively. The values w_{odd} and w_{even} are equal to 1.3 and 1, and were chosen such as to yield position invariance in the complex cell receptive field. This could be interpreted either as the relative presence of the two phases in the cortex, or as the result of different synaptic strengths due to Hebbian learning.

There are 3200 complex cells in the model (2 x 40 x 40), arranged in two groups, one comprised of large inhibitory cells and the other of small excitatory cells. Each excitatory complex cell receives input from the four corresponding small-RF simple cells, and each inhibitory complex cell receives input from the four corresponding large-RF simple cells. Both groups are arranged according to the same orientation preference map as the simple cells. The area that contains complex cells is confined to the central 40 x 40 grid of the 64 x 64 grid of the simple cell orientation map in order to eliminate edge

effects. Complex cells in the model fire with a baseline firing rate (i.e., the response of the cell in absence of the stimulus, when presynaptic inputs are at baseline level) of 10.7 Hz. This value is within the range found experimentally in both cat and macaque (Katzner et al. 2011, Ringach et al. 2002). The baseline firing rate of all subsequent cell types in the model is also 10.7 Hz.

3.2.4 End Stopped Cells

The third stage of the model is comprised of 1600 (40 x 40) end-stopped cells. End-stopped cells are orientation-tuned and have been recorded in V1 and V2. The term end-stopped comes from the fact that their responses are suppressed for stimuli that extend beyond an optimal bar length. Each end-stopped cell receives input from excitatory and inhibitory complex cells with matching preferred orientations and receptive field centers, as suggested by (Hubel and Wiesel 1965). The receptive fields of the excitatory complex cells are smaller than those of the inhibitory complex cells, which results in end-stopped behavior. This type of inhibitory input could be provided by complex cells from layer 6 (Bolz and Gilbert 1986). The firing rate of end-stopped cells is defined by Eq. 4.

$$R_{es} = [w_{ex}R_{C,ex} - w_{inh}R_{C,inh} - \theta]_+ + R_{C,bl} \quad \textbf{(4)}$$

where R_{es}, $R_{C,ex}$, and $R_{C,inh}$ refer to the firing rates of end-stopped, complex excitatory,

and complex inhibitory cells, respectively. The terms w_{ex} and w_{inh} are the relative weights of the inputs from excitatory and inhibitory cells to end-stopped cells, and are equal to 3.5 and 1.3, respectively. These values have been selected to optimally reproduce experimentally observed end-stopping behavior. The lower weight for the inhibitory cells allows the sum of inputs to the end-stopped cell to be positive for stimuli placed in the center of the receptive field. $R_{C,bl}$ is the baseline firing rate of complex cells, and θ is the threshold input necessary to evoke a response, defined by the equation $\theta = R_{C,bl}(w_{ex} - w_{inh})$.

One important consideration when modeling end-stopped cells is the response to stimuli that are not exactly of the preferred orientation. The receptive field of an end stopped cell is typically described as an excitatory central region with inhibitory end regions. This results in a response that is diminished as the stimulus length is increased beyond the optimal amount. However, when developing a model for end-stopped cells, it was found that a model that takes into account only an excitatory center with inhibitory ends produces false positive responses for long stimuli that are slightly off from the correct orientation. This type of false positive response is not seen experimentally, as end-stopped cells are inhibited by long bars of all orientations. In order to solve this problem, we have introduced what has been referred to as side-stopping, or side inhibition, that is, inhibitory side regions as well as end regions. There is experimental evidence for side inhibition that makes this a plausible explanation (Blakemore and Tobin 1972; Bishop, Coombs and Henry 1973; Maffei and Fiorentini 1976; Nelson and Frost 1978; Orban, Kato and Bishop 1979; Morrone, Burr and Maffei 1982; De Valois, Thorell and Albrecht 1985; Allman, Miezin and McGuinness 1985). In the model, it is accomplished by providing inhibition from cells whose receptive fields are both wider

and longer than the cells that provide excitation.

3.2.5 Topographic organization of V1 cells

The topographical arrangement of V1 cells in the model is characterized by a non-homogeneous orientation map generated so as to correspond to those observed experimentally (Hubel et al. 1978; Blasdel et al. 1986; Grinvald et al. 1986). The same orientation map is used for each V1 cell type, and is modeled using the techniques described in (Kohonen 1982). Each neuron is characterized by a unique set of (x,y,θ) coordinates, where (x,y) is the retinotopic position and θ is the cell's preferred orientation. There are 16 possible preferred orientations for the model neurons, spanning the range $[0°, 180°]$. The orientations are evenly distributed across the model cortex. For V2 cells, all orientations are uniformly distributed across the visual field.

3.2.6 Pattern cells

The fourth stage of the model consists of cells that respond to both real and illusory contours. These cells will be referred to within this paper as pattern cells. Pattern cells represent a known cell type observed primarily in V2 that exhibit orientation tuning for both real and illusory contours (Von der Heydt and Peterhans,1989; Sheth et al., 1996).

In the model, the pattern cells are organized in 16 groups, each group with a

distinct orientation preference, altogether uniformly covering the range from 0-180 deg. They receive input from complex excitatory cells and end-stopped cells. Complex excitatory cells provide input if their orientation is parallel or nearly parallel to the preferred orientation of the pattern cells and their center is located within a tolerance Δxc from the main axis of the pattern cell receptive field. End-stopped cells provide input if their preferred orientation is orthogonal or nearly orthogonal to the preferred orientation of the pattern cells and the position of the end of their receptive field is located within a tolerance Δxe from the main axis of the pattern cell receptive field. End-stopped cells are responsible for a pattern cell's ability to respond to illusory contours. To ensure that a pattern cell responds correctly, the topographic position of end-stopped cells providing input must be more precise than that of the complex cells, resulting in a smaller tolerance. As a consequence, the cortical area providing input from end-stopped cells is one fifth the size of the cortical area providing input from complex cells. In order to compensate for this discrepancy, we allow a wider orientation tolerance for the end-stopped cells providing input. This means that a wider set of end-stopped cell orientations are involved in calculating the connectivity matrix from end-stopped cells to pattern cells. To ensure that no distortions occur in the quadratic exponential when, due to the broader range of inputs, the difference in preferred orientation between pattern cells and end-stopped cells exceeds 180 degrees, we use a cosine function. Based on these considerations, the connectivity weights are given by the following equations:

$$mp_{ES}(i,j) = e^{-5\cos(\theta_i - \phi_j)^2} H_{ES}(\mathbf{re}_i, \mathbf{rp}_j) \qquad \textbf{(5)}$$

$$mp_{Exc}(i,k) = e^{\frac{-(\theta_i - \phi_k)^2}{\sigma_\theta^2} + \frac{-(\mathbf{rc}_i - \mathbf{rp}_k)^2}{\sigma_{pos}^2}} H_{Exc}(\mathbf{rc}_i, \mathbf{rp}_k) \qquad \textbf{(6)}$$

where mp_{ES} and mp_{EXC} are matrices that define the connections to pattern cell *i* from end-stopped cell *j* and from excitatory complex cell *k*, respectively. The parameter θ_i is the preferred orientation of the pattern cell, ϕ_j is the preferred orientation of the end-stopped cell, and Φ_k is the preferred orientation of the complex cell. The vectors **re**, **rc**, and **rp** denote the positions of the end-stopped, complex, or pattern cells, respectively on the topographical map of the cortex, relative to the center of the visual field of the postsynaptic neuron. The parameters σ_θ and σ_{pos} are the standard deviations in preferred orientation and position and characterize the exponential decrease in the strength of connections to pattern cells from complex cells as the position and orientation of the latter deviate farther from the main axis of the pattern cell receptive field. They are equal to 0.2 deg and 1 deg, respectively.

The functions H_{ES} and H_{Exc} are connectivity templates taking values 0 or 1, and are designed to restrict input to pattern cells to: 1) end-stopped cells whose ends terminate along the axis of the pattern cell's receptive field, and 2) complex excitatory cells whose receptive fields are collinear with the pattern cell's receptive field axis. For end-stopped cells, this is the only position dependent component of the connection matrix. In the case of complex cells, this function provides a spatial cut-off. They are

given by the following expressions for a vertical preferred orientation:

$$H_{ES} = [\Theta(\overline{xe}_j - xp_i - \frac{\Delta xe}{2}) - \Theta(\overline{xe}_j - xp_i + \frac{\Delta xe}{2})] \times [\Theta(ye_j - yp_i - \frac{L_P}{2}) - \Theta(ye_j - yp_i + \frac{L_P}{2})]$$

$$H_{Exc} = [\Theta(xc_k - xp_i - \frac{\Delta xc}{2}) - \Theta(xc_k - xp_i + \frac{\Delta xc}{2})] \times [\Theta(yc_k - yp_i - \frac{L_P}{2}) - \Theta(yc_k - yp_i + \frac{L_P}{2})]$$

$$\Theta(x) = \begin{cases} 0, x < 0 \\ 1, x \geq 0 \end{cases}$$

where a bar above *xe* denotes the position of the end of the end-stopped cell's receptive field rather than its center, Δxe and Δxc are the allowed variation in *x*-position of end-stopped and complex excitatory cells (0.1 deg and 1 deg, respectively), and L_p is the length of the footprint of the pattern cell receptive field (4 deg) (Hubel and Wiesel 1965). Expressions of these functions for all other preferred orientations are obtained by Cartesian rotation.

The firing rate of pattern cells in our model is given by:

$$R_{Pat} = \left[mp_{ES} \cdot R_{ES} + mp_{Exc} \cdot R_{Exc} - \gamma \right]_+ \qquad \textbf{(7)}$$

where R_{ES} and R_{Exc} are vectors representing the firing rates of end-stopped and complex excitatory cells, respectively, and γ is the threshold for response and is defined by the

equation $\gamma = R_{C,bl}(mp_{ES}+mp_{Exc}-1)$.

Preliminary pattern cell characterizations will be discussed here, while further results will be the focus of Chapter IV.

3.2.7 Classifier units (V4/IT)

The final stage of processing in the model consists of cells capable of performing a figure-ground separation task. This layer of the model will be the focus of Chapter V, and will be described in detail there.

3.3 Model tuning

Our model reproduces important aspects of known cell types at every stage of processing. We will first compare typical V1 cell properties with the responses of the neurons at the V1 stage of our model. Then we will investigate potential mechanisms for the known properties of pattern cells.

3.3.1 Simple Cells

Simple cells are found in area V1 (Hubel and Wiesel 1965). A typical simple cell is orientation tuned, and is preferentially activated by one of the following types of stimuli: bright bars on a dark background, dark bars on a bright background, or bright-

dark edges. To assess the functionality of the simple cell stage of the model, we tested it for orientation tuning using bright and dark bars at 16 different orientations. Figure 3.2 shows an average tuning curve across four individual simple cells (all with the same size of receptive field) that prefer bright bars on dark background, whose receptive field centers are within 0.1 degrees of visual field from the center of the stimulus. A similar tuning curve was obtained for simple cells preferring dark bars on a bright background (results not shown). These orientation tuning properties closely resemble those observed experimentally (Hubel and Wiesel 1965).

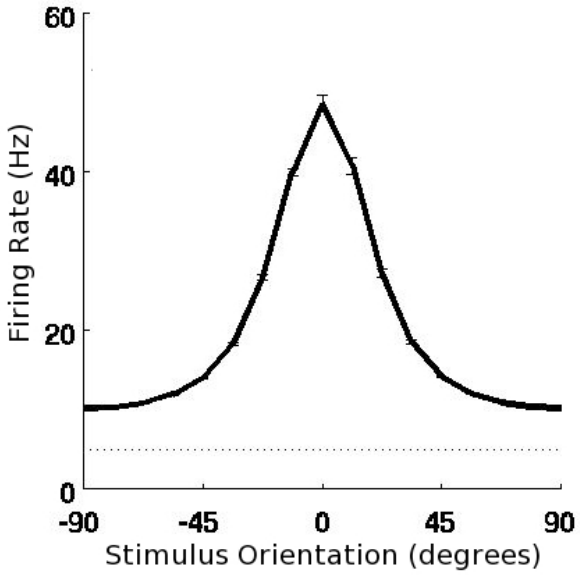

Figure 3.2 Tuning curve of simple cells in the model. The curve was obtained by averaging over all simple cells with the RF in the center of the visual field. The half-height tuning width is 40.7 degrees. The dotted line reflects the baseline activity of simple cells in the model.

Additionally, the simple cells in the model exhibited phase- and position-preference. For example, ON-OFF-ON cells responded strongly to a dark bar on a bright

background when the bar was centered on the OFF-subfield, but they were inhibited when the bar was moved to one of the ON-subfields, or when the contrast was inverted (results not shown). The position preference was sharply tuned: activation was maximum when the stimulus was centered on the receptive field of the cell, and it decreased with a steep slope as the stimulus moved away from the receptive field center in a direction perpendicular to the preferred orientation (dotted line in Figure 3.4). Simple cells in the model have a tuning width at half-height of 40.7 degrees, which is within the range of 10 to 50 degrees observed in cat by (Heggelund and Albus 1978).

3.3.2 Complex Cells

The defining characteristics of complex cells that we aimed to reproduce were orientation tuning, position invariance, and phase invariance (Hubel and Wiesel 1962, Movshon et al. 1978). We tested orientation tuning using the method described above for simple cells and found that complex cells in the model exhibited orientation tuning as well (Figure 3.3). Complex cells in the model have a tuning width at half height of 38.9 degrees.

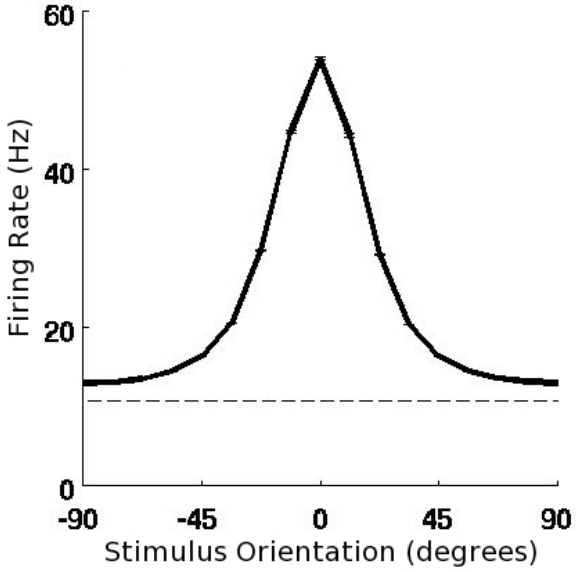

Figure 3.3 Tuning curve of complex cells in the model. The curve was obtained by averaging over all complex cells with the RF in the center of the visual field. The half-height tuning width was 38.9 degrees. The dashed line reflects the baseline activity of complex cells in the model. In both A and B, the error bars represent the standard error of the mean.

To measure position invariance, we moved a bar of the preferred orientation across the receptive field of a complex cell (Figure 3.4, solid line). The complex cell maintained a near-maximum response over a range of positions spanning approximately half a degree, more than twice that exhibited by simple cells.

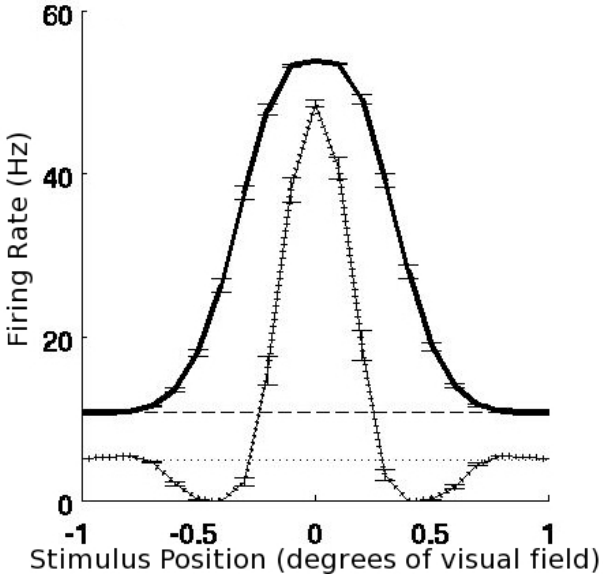

Figure 3.4 Position invariance in complex cells. Solid line shows the response of a sample complex cell to a translated bar. The response of a simple cell to the same stimulus is shown with the dashed line, for comparison. The half-height width is 0.3 degrees for simple cells and 0.7 degrees for complex cells.

We performed orientation tuning and position-invariance tests with both bright and dark stimuli and obtained identical results (not shown), confirming that the complex cells in the model were phase invariant.

3.3.3 End-Stopped Cells

End-stopped cells are a type of complex cell whose responses vary nonlinearly with the length of the stimulus. More precisely, their responses increase with stimulus length up to a certain threshold, after which they decrease with increasing stimulus length as long as the stimulus is within the cell's receptive field (Hubel and Wiesel 1965, Bolz

and Gilbert 1986).

To determine whether the cells in the model displayed end-stopping behavior, we measured the cell's firing rate for a bar of the preferred width and orientation as the length of the bar was increased (Figure 3.5). As expected, the cell's firing rate increased with length up to a certain point, beyond which it decreased to baseline. Based on this graph, we found that the preferred bar length for end-stopped cells in the model was 1.2 degrees of visual field.

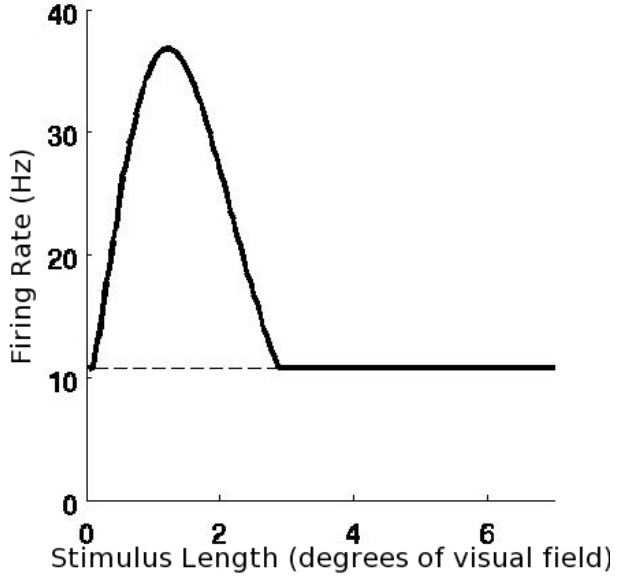

Figure 3.5 Preferred stimulus length of an end-stopped cell. The figure shows the response of an end-stopped cell as the length of the stimulus is increased.

3.3.4 Pattern Cells

Pattern cells in our model are intended to reproduce the behavior of cells in V2

that respond to both real and illusory contours, such as those found experimentally (Von der Heydt and Peterhans 1984; Von der Heydt and Peterhans 1989). These cells are tuned to real and illusory contours of the same orientation, although the shapes of the tuning curves vary widely (Von der Heydt and Peterhans, 1989). In some cases they are identical for both stimulus types, but in others, the tuning curve for one type of stimulus may have a higher or lower peak, a larger or narrower tuning width, or even a slight shift in preferred orientation.

Single cell response

Figure 3.6 shows tuning curves of three sample V2 cells from the model whose receptive fields are near the center of the visual field. The solid line represents the response to real contours and the dashed line represents the response to illusory contours. The graphs indicate that the pattern cells in our model are orientation tuned for both real and illusory contours. Therefore illusory contour detection can be obtained using a simple feed-forward mechanism even when realistic V1 orientation maps are taken into account.

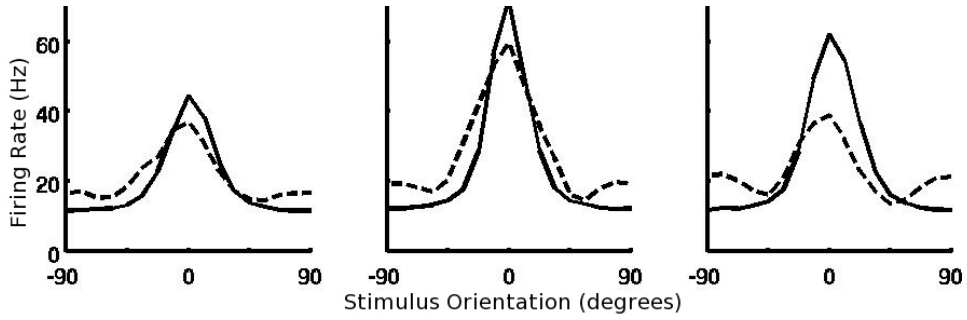

Figure 3.6 Tuning curves for real (solid line) and illusory (dashed line) contours of four sample pattern cells. The cells were selected such that the stimuli were in the center of their receptive fields. Both real and illusory contours were the same length (full field). The average value the peak-to-trough distance was 42±9 Hz for real contours and 27±10 Hz for illusory contours.

Population response

We validated the responses of the model at population level by reproducing the results from two imaging experiments: Sheth et al 1996, and Ramsden et al 2001.

Sheth et al. looked at activation in areas V1 and V2 in response to real and illusory contours, and developed a map based on which orientation evoked the highest response at a given location (Refer to section 2.3.2 for more information). They looked at the difference in the maps for real and illusory contours. Their premise was that if the difference in preferred orientation for real and illusory contours is near 0 degrees, that section of the cortex responds to illusory contours, while if the difference in preferred orientation is near 90 degrees, it responds only to the inducing lines.

Figure 3.7 shows that complex cells in the model reproduce population level results observed at the level of V1: the difference in preferred orientation for real and

illusory contours is primarily closer to 90 degrees, indicating that cells respond only to the inducing lines.

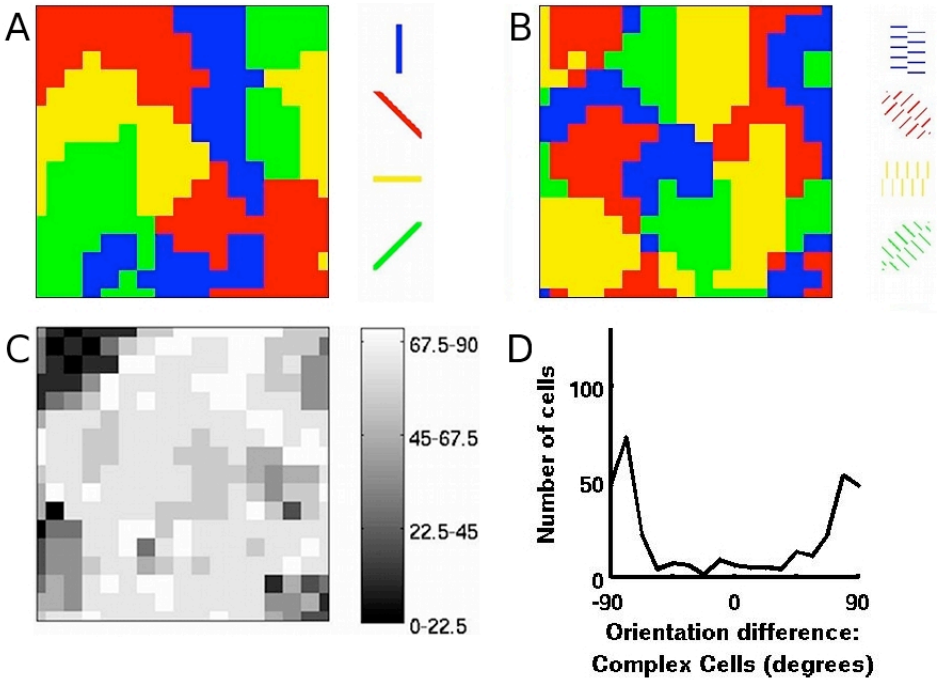

Figure 3.7 Reproduction of Sheth et al. (1996) experimental results at the level of V1. A) Each pixel represents a single complex cell in the model. The color of each pixel indicates the real contour orientation that evokes the highest activation for each cell. B) Illusory contour orientation that evokes the highest activation. C) Map of the difference between A and B. D) Histogram of values in C. Because the peak of this graph is at 90 degrees, these cells do not respond to illusory contours.

Figure 3.8 shows that pattern cells in the model can reproduce population-level results measured in V2: the difference in preferred orientation is 0 degrees, indicating that the cells respond to the orientation of the illusory contour, and not the inducing lines.

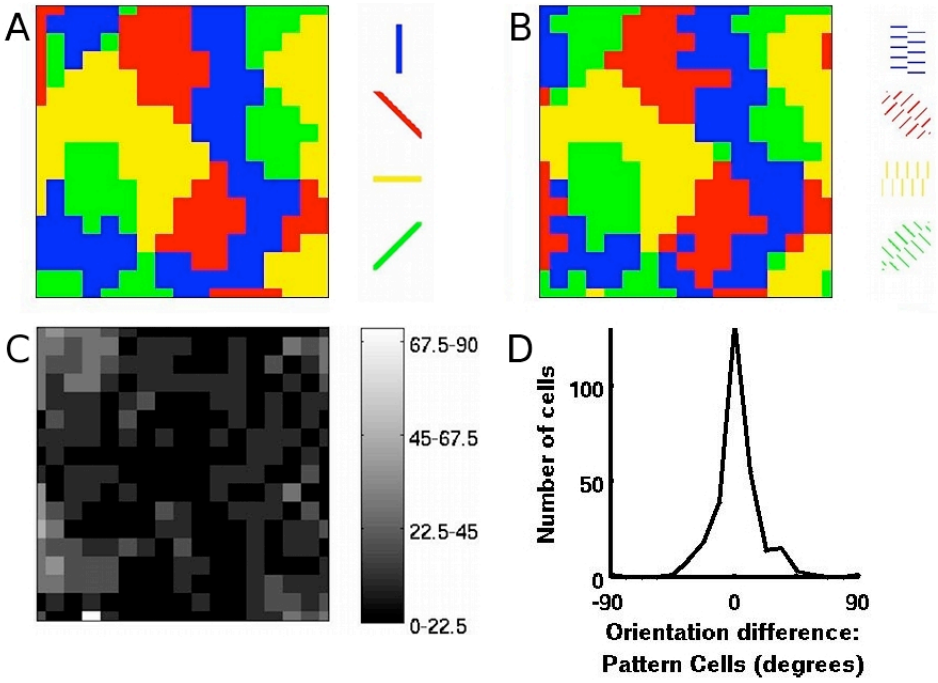

Figure 3.8 Reproduction of Sheth et al. (1996) experimental results at the level of V2. A) Each pixel represents a single pattern cell in the model. The color of each pixel indicates the real contour orientation that evokes the highest activation for each cell. B) Illusory contour orientation that evokes the highest activation. C) Map of the difference between A and B. D) Histogram of values in C. Because the peak of this graph is at 0 degrees, these cells respond to the orientation of illusory contours, rather than to the orientation of the inducing lines

We were also able to reproduce the results of (Ramsden et al. 2001), which showed that in V2, the same areas were most highly activated in V2 for both real and illusory contours of the same orientation (Figure 3.9), while in V1, the areas that are most highly activated for vertical real contours were most highly activated for horizontal illusory contours, and vice versa (Figure 3.10). One limitation of the model is that it does not respond well to illusory contours with inducers slanted at 45 degrees. As such, we

used illusory contours with orthogonal inducers and were therefore unable to eliminate the response to inducers at the level of V1. For this reason, the V1 responses in the model should be interpreted as evidence that our model's V1 area responds to inducers rather than illusory contours. This would imply that the responses observed at V1 level by Ramsden et al. (2001) cannot be explained using a purely feed-forward mechanism, and that feedback from V2 area is required.

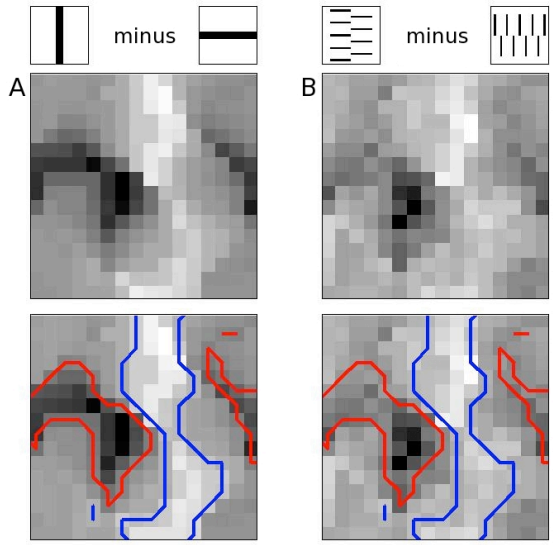

Figure 3.9 Reproduction of Ramsden et al. (2001) experimental results at the level of V2. The areas that are most highly activated for vertical real contours (A, white regions) the same areas that are most highly activated for vertical illusory contours (B, white regions). On both plots, the areas that are most highly activated for vertical real contours are outlined in blue, while the areas that are most highly activated for horizontal real contours are outlined in red.

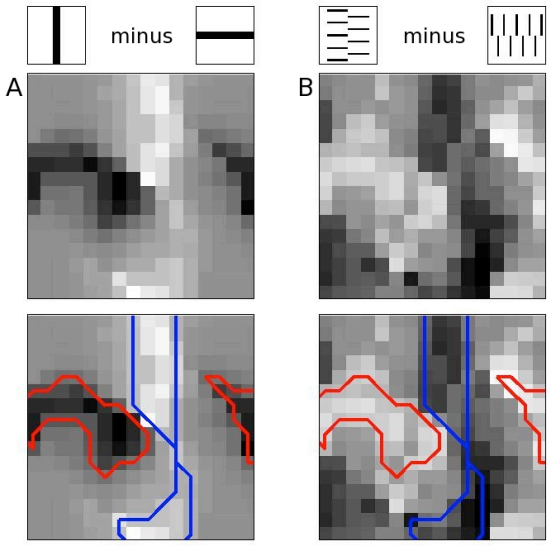

Figure 3.10 Reproduction of Ramsden et al. (2001) experimental results at the level of V1. The areas that are most highly activated for vertical real contours (A, white regions) are the areas that are most highly activated for horizontal illusory contours (B, black regions). On both plots, the areas that are most highly activated for vertical real contours are outlined in blue, while the areas that are most highly activated for horizontal real contours are outlined in red.

Pattern cell response validation

Before we use the model to investigate the properties of pattern cells, we need to address three important questions. First, do the model cells in fact respond to illusory contours, or is the same response produced by any distribution of parallel bars? Second, is the response of the model robust to noise? And finally, how plausible is the proposed cortical circuitry?

We begin with the question of whether our model truly responds to illusory contours, or whether it responds simply to a distribution of parallel bars. To this end, we altered an illusory contour by shifting the position of each inducer by a random amount

along its length, up to a value of half the length of the inducer. We repeated this process six times, and constructed an average curve (Figure 3.11, red line). We subsequently increased the magnitude of the maximum shift up to the full length of the inducer (Figure 3.11, blue line). We observe that the amplitude of the tuning curve decreases as the magnitude of the shift increases. Additionally, the peak of the tuning curve for an illusory contour (Figure 3.11, black line) is at least 40% higher than that corresponding to any other distribution of inducers. This indicates that the response we observe in V2 cells in our model is a response to illusory contours, and not merely to an arrangement of parallel lines.

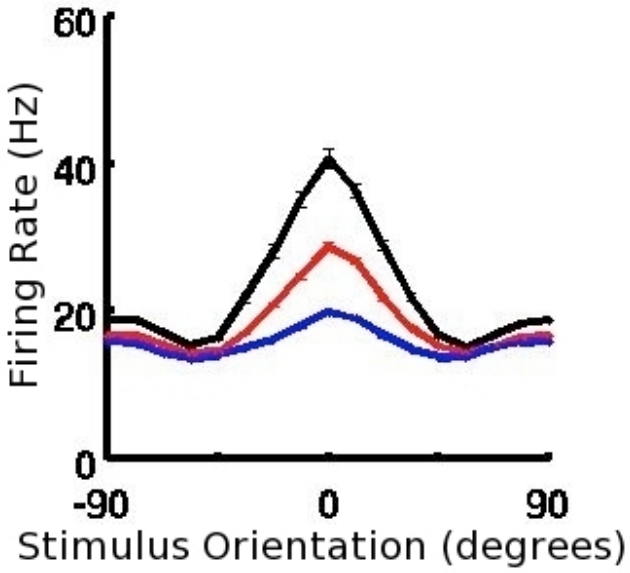

Figure 3.11 Response of model V2 cells to illusory contours when inducers are misaligned with respect to the illusory contour. Tuning curves are built when the position of the inducing lines is randomly shifted by 0 deg (black), 0.5 deg (red), and 1 deg (blue). As the image ceases to be an illusory contour, the response drops to almost baseline.

The next question is whether this mechanism would continue to detect illusory contours in biologically realistic circumstances, i.e., when noise is present. To simulate such circumstances, we applied noise to the V1 simple cells in the form of a uniformly random input to each cell ranging between -5 and +5 Hz with an average of 0 Hz. This noise propagated downstream to all cell types. Figure 3.12 shows tuning curves for real and illusory contours in this condition (red curves) compared with the situation in which no noise is present (black curves). We note that there is no statistically significant difference between these curves in the 45 degree interval centered on the preferred orientation (one way ANOVA, $p>0.01$).

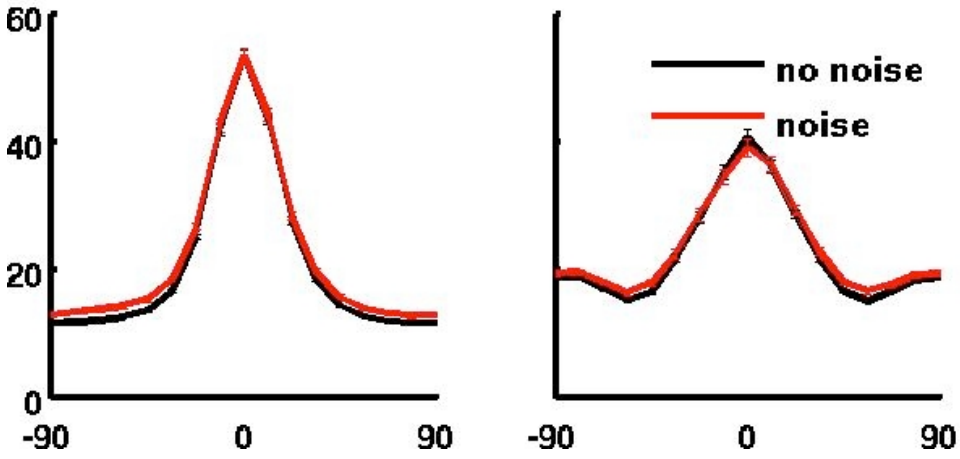

Figure 3.12 Robustness to noise. Tuning curves for real (left panel) and illusory (right panel) contours are not affected when up to 10 Hz noise is applied to the simple cells (red curve vs black curve).

Finally, the ability of the pattern cells in our model to respond to illusory contours arises from the connectivity scheme between the V1 complex and end-stopped cells and the V2 pattern cells (Figure 3.13 A). But is such neural circuitry biologically plausible?

While a precise mapping of connections between V1 and V2 cells has not yet been determined experimentally, there is data that allows us to infer these connections. Anzai et al. (2007) found that some V2 receptive fields exhibit a fine structure, i.e. the center of the receptive field has a different orientation preference compared with the periphery (Figure 3.13 B, upper panel). Such behavior is indicative of presynaptic inputs arriving to the V2 cell from V1 cells with at least two different orientation preferences, similar to the circuitry in our model. Indeed, when exploring the fine structure of our pattern cell receptive fields, using a similar paradigm as in Anzai et al, we detect a similar receptive field structure (Figure 3.13 B, lower panel). The experimental results establish the feasibility of the hypothetical circuit.

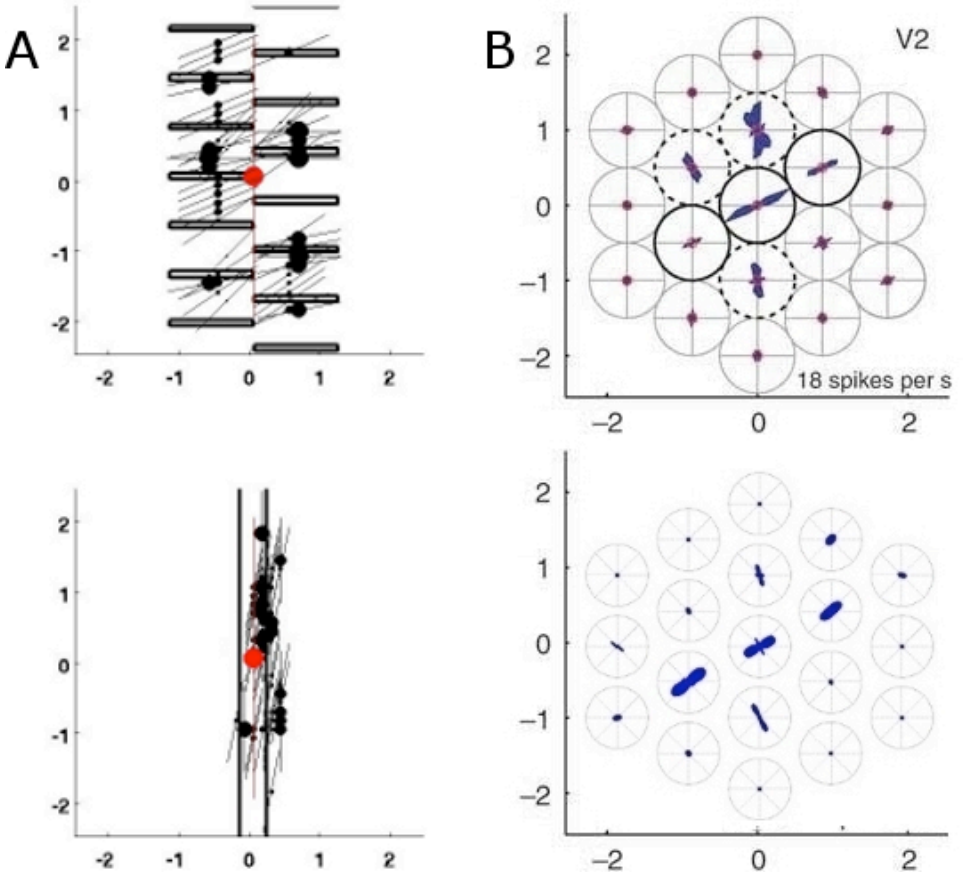

Figure 3.13 Variability in connections and plausibility of proposed circuitry. A) Snapshot of connections to a sample V2 cell. The red point represents a single V2 pattern cell. Each black dot represents an end-stopped cell (upper panel) or a complex cell (lower panel) that provides input to this pattern cell. The size of each black dot indicates the relative connection strength, and the line going through it shows the position and orientation of the cell's receptive field. The stimulus responsible for activating each set of connections is superimposed. The connections are not homogenously distributed across the cortical area due to the non-uniform nature of the orientation preference map for the V1 cells. B) Plausibility of circuitry. The neuronal circuit we propose produces a receptive field fine structure (lower panel) similar with that observed experimentally (upper panel, Anzai et al. 2007). The receptive field was investigated by using a dark bar 1 deg long and 0.3 deg wide that was placed in different locations of the pattern cell receptive field as shown. Each polar plot represents the firing rate of the pattern cell as a function of the orientation of the bar.

3.4 Conclusion

In order to study various aspects of illusory contour detection, we have developed a computational firing-rate model that contains cell types hypothesized to play a role in this process. The model consists of four stages of processing, which are denoted as simple, complex, end-stopped, and pattern cells. Each of the four stages of the model correctly reproduces the behavior of corresponding cells in the visual cortex. In particular, pattern cells in the model exhibit responses to real and illusory contours that correspond to the experimentally observed behavior of V2 cells. Additionally, the orientation tuning curves that we obtained for real and illusory contours for V2 cells in our model closely resemble those observed experimentally. We verified that the model is robust to noise and that the response to illusory contours cannot be explained by mere presence of random distribution of parallel gratings.

Limitations of the model

Computational power considerations as well as a desire to keep the model as simple as possible led us to limit the number and type of neurons in the model to the minimum necessary. For this reason, our model does not include any T-junction cells, which are considered essential in the detection of amodal illusory contours (Kanizsa figures), hence cells in our model will not respond to such contours.

We will further use this model to explore important aspects related to illusory contour detection, as well as effects of injuries in primary visual cortex on early visual cognition.

Chapter IV

Detection of illusory contours: The influence of V1 cell properties on V2 cell response

4.1 Introduction

Using the model described in Chapter III, we are able to examine single-cell responses and show the following: a) illusory contour detection can be achieved even when considering a realistic organization of V1 neurons according to orientation preference maps, b) inducer spacing preference is determined by the distribution of receptive field sizes in the synaptic input from V1, c) response to illusory contours with non-orthogonal inducers depends on the spectrum of orientation preferences of the end-stopped cells providing input to the V2 cell. The model also allows us to tackle more complex questions, such as the relationship between the contrast response functions for real and illusory contours, and the effect of a small cortical injury in V1 on the response properties of downstream neurons.

4.2 The model

Refer to section 3.2.

4.3 The stimuli

Refer to section 3.2.1

4.4 Results

4.4.1 Response of V2 cells to illusory contours

In general, computational modeling and experimental data differ in that model cells belonging to a single type display identical properties while experimentally observed cells of the same type exhibit a wide range of behaviors. In our model, as in experiment, cells exhibit response variability (see Figure 3.6). Within the model, this is determined by the orientation map of the pre-synaptic neurons. More specifically, the total strength of connections from end-stopped and complex cells to pattern cells is dependent on the local availability of pre-synaptic cells of a particular orientation and position preference (as an example, refer to Figure 3.9). Due to the non-homogenous nature of the orientation map, the total strength of all pre-synaptic connections to pattern cells is not a constant, giving rise to the observed variability in tuning curves. In order to quantify this effect, we ranked the pattern cells in the center of the visual field as a function of the total strength of connections from complex cells (for real contour response) and end-stopped cells (for illusory contour response). Next, we averaged separately the tuning curves for the pattern cells that received a total connection strength

within the upper or lower quartile (black and red lines respectively, in Figure 4.1). We found that the heterogeneity of the orientation map can cause a change of up to 60% in the amplitude of the tuning curve for illusory contours and 40% for real contours without affecting the tuning width.

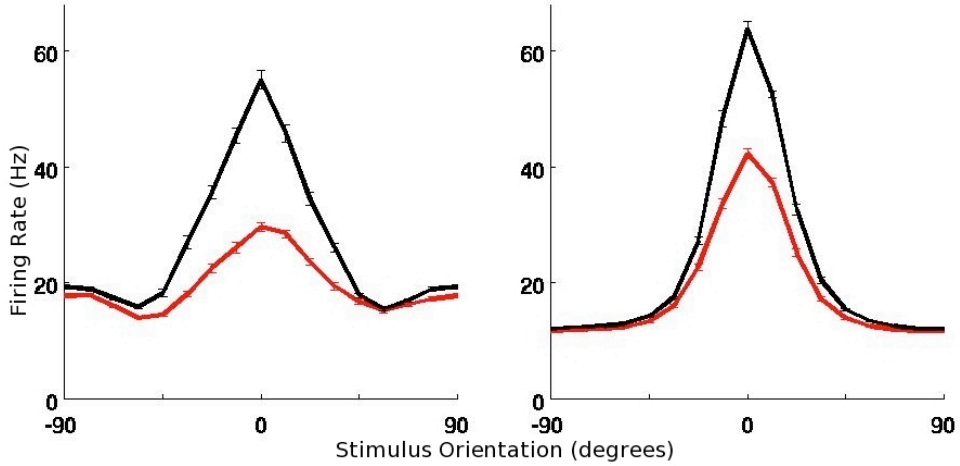

Figure 4.1 Variations in the tuning curve shapes are a direct consequence of heterogeneity in the orientation map in V1. In response to the presentation of illusory contours (upper panel), V2 cells with greater total synaptic strength to end-stopped cells have a higher amplitude tuning curve (black line, peak-to-trough=40 Hz) than V2 cells with smaller total synaptic strength to end-stopped cells (red line, peak-to-trough=16 Hz). A similar effect is present for real contours as a function of total synaptic strength from complex cells to pattern cells (lower panel, black line peak-to-trough= 52 Hz, red line peak-to-trough=31 Hz)

4.4.3 Inducer spacing preference in V2

We examined the dependence of V2 cell responses on the spacing between inducers in the abutting grating stimulus. Such dependence has been investigated experimentally by (Von der Heydt and Peterhans 1989) using abutting gratings with

increasing distance between the inducing lines. They found both cells that had an optimal inducer spacing and cells that showed a largely unchanged response across a range of inducer spacings. Using a similar paradigm, we determined that all V2 cells in our model were sharply tuned for an inducer spacing of 0.7 degrees (Figure 4.2).

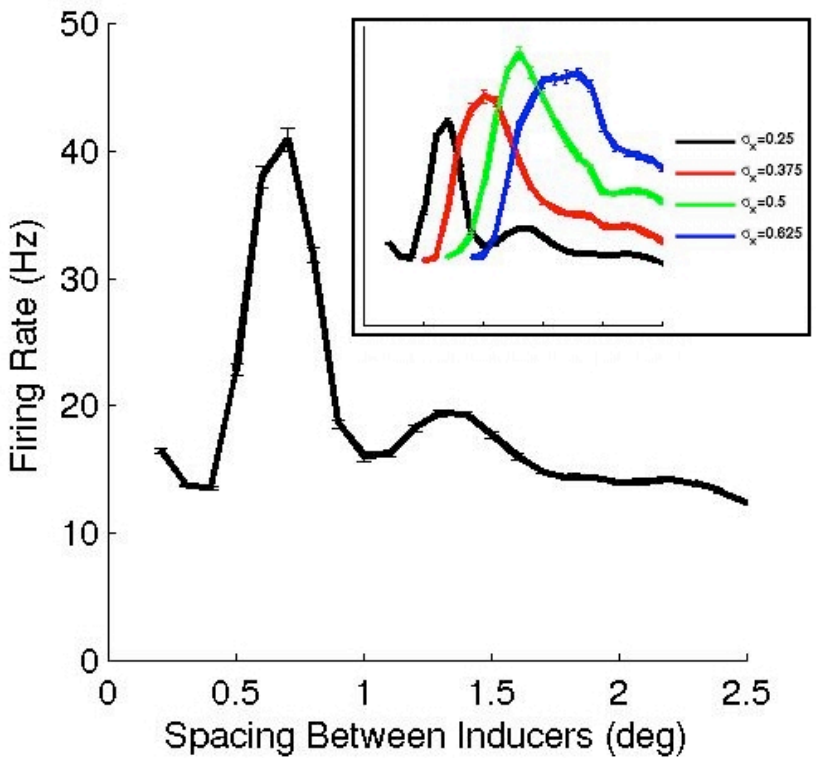

Figure 4.2 Dependence of illusory contour response on inducer spacing. The figure shows the average response of 40 cells (whose receptive fields were centered on the illusory contour) to abutting grating stimuli with 25 different inducer spacings. The preferred inducer spacing in the model was 0.7 degrees of visual field. Inset: Same average for four different widths of simple cell receptive fields.

The similarity between this width and the width of the simple cell receptive fields in the model led us to hypothesize that the two were related. To validate this hypothesis, we calculated the response of pattern cells to stimuli with different inducer spacings,

while at the same time varying the size of the model simple cell receptive fields. We found that the preferred inducer spacing increased proportionally to the simple cell receptive field width (Figure 4.2, inset). By looking at the correlation between the preferred inducer spacing and the width of the simple cell receptive subfields (Figure 4.3), we were able to quantify this dependence as

$$IS_{preferred} = 1.67 \times W_{subfield}$$

where $IS_{preferred}$ is the preferred inducer spacing for a given pattern cell and $W_{subfield}$ is the subfield width for the simple cells presynaptic to that pattern cell. This leads us to conclude that the experimentally observed dependence on inducer spacing is a reflection of the distribution of the receptive field widths of presynaptic neurons. A distribution strongly biased towards one particular receptive field width results in cells that have a preferred inducer spacing, while a broader distribution of receptive field widths produces cells that respond similarly to a range of inducer spacings.

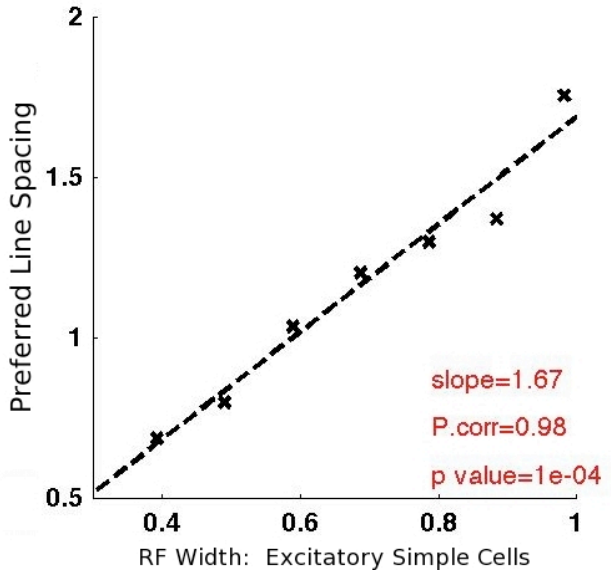

Figure 4.3 Correlation between the preferred inducer spacing of pattern cells and the simple cell receptive subfield width. The preferred inducer line spacing is 1.67 × simple cell receptive subfield width (correlation coefficient 0.99, p=0.0001)

4.4.4 Effect of inducer angle relative to the illusory contour on V2 cell response

Experimentally, it has been found that when cells are shown illusory contours whose inducers are not orthogonal to the contour, they respond in one of two ways: some cells respond to the orientation of the illusory contour regardless of the orientation of the inducers, while others signal an orientation that is shifted away from the orientation of the illusory contour, towards the orientation orthogonal to the inducers (Von der Heydt and Peterhans 1989). We studied the influence of the angle between the inducing lines and the illusory contour on the response elicited from V2 cells in the model. To this end, we used three different illusory contours: one with orthogonal inducers and two with inducers at angles of 79 and 101 degrees to the illusory contour. For the two stimuli with

non-orthogonal inducers, we obtained tuning curves that were shifted towards the orientation orthogonal to the inducers (Figure 4.4, left panel). In our model, the input that a pattern cell of a given orientation preference receives from an end-stopped cell with an orthogonal orientation preference is at least 20% stronger than the input from any other individual end-stopped cell. This leads us to the hypothesis that peak shift for non-orthogonal inducers is due to the reduced connection strength from presynaptic end stopped cells with orientation preferences not orthogonal to the pattern cell's preferred orientation. The direct implication is that uniform connection strength over a range of preferred orientations in the input would yield pattern cells whose response is largely invariant to the angle of the inducers with respect to the illusory contour. We verified this hypothesis by building pattern cells whose input was provided by end stopped cells with preferred orientations anywhere in the range (-60,60) degrees at equal connection strengths (right panel in Figure 4.4). Indeed, the tuning curves of such cells showed little sensitivity to the angle of the inducers. These two connectivity schemes explain both types of behavior observed experimentally.

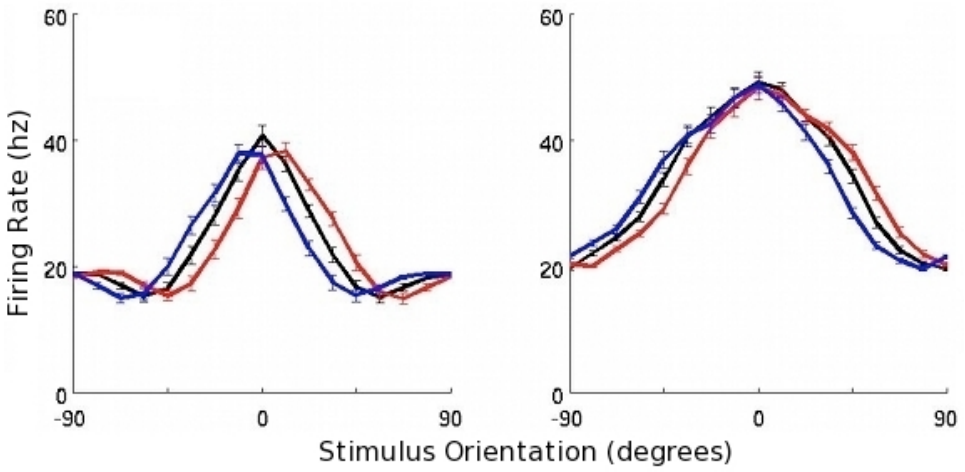

Figure 4.4 Orientation tuning when inducer angles are not orthogonal to the illusory contour. The tuning curves are shifted towards the orientation orthogonal to the inducers. Red and blue lines correspond to inducers with the orientation shifted π/16 radians (11.25 degrees) clockwise and counterclockwise, respectively. For reference, we provide a tuning curve for an illusory contour with orthogonal inducers (black line). The left panel reflects a situation in which the strength of the connections from end-stopped cells to pattern cells is strongest when the two cells have orthogonal orientation preferences. The right panel reflects an arrangement in which all end-stopped cells whose ends are in an appropriate position and whose orientation preferences are between +/-60 deg of the orientation orthogonal to the preferred orientation of the pattern cell, provide equal input.

4.4.5 Contrast Response Function

We determined the contrast response function of the pattern cells in our model for real and illusory contours. More specifically, we were interested in whether there were any differences between the contrast response curves, and if so, what the differences were. In order to better isolate the impact that the proposed cortical circuitry would have on contrast response function, we did not implement any contrast saturation mechanisms at the level of LGN and retinal ganglion cells in our model, hence we do not expect contrast saturation in our curves from these sources. To construct the contrast response

functions of pattern cells in the model, we used real and illusory contours at ten different contrast values. The left panel in Figure 4.5 shows the contrast response function for real (red) and illusory (blue) contours. It is easy to observe that at low contrast, the response to illusory contours increases at a slower rate than to real contours. This trend becomes clearer when the derivative of the contrast response function is plotted (right panel of Figure 4.5). The main difference between processing illusory contours and real contours, according to the circuitry proposed in this model, is that in the case of illusory contours there is an extra step, as visual information passes through end-stopped cells before reaching pattern cells. Hence, experimental observation of such contrast response function behavior for real and illusory contours would be consistent with the hypothesis that end-stopped cells form an obligatory in illusory contour detection.

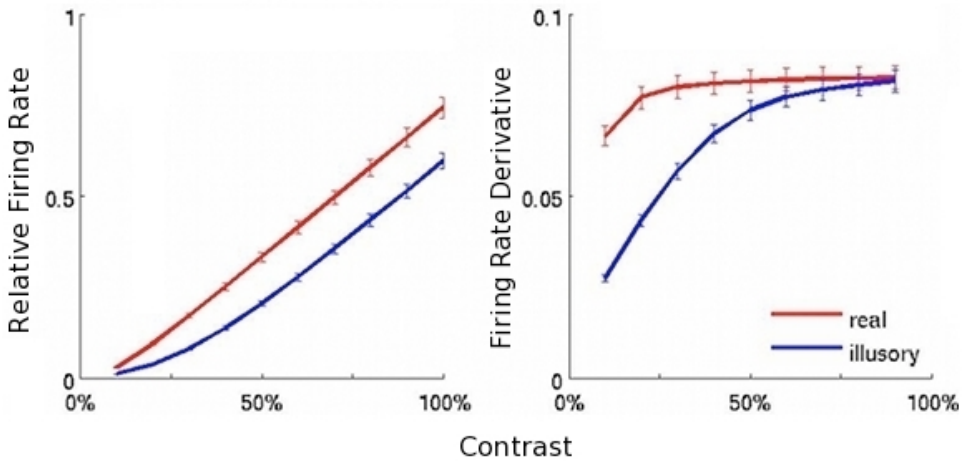

Figure 4.5 Difference in contrast response function and its derivative for real and illusory contours. The left panel shows the contrast response function and the right panel shows the derivative of the contrast response function. Red lines indicate real contours and blue lines indicate illusory contours. Note that real contours elicit stronger responses than illusory contours at a given contrast value. Also, the response as a function of contrast for real contours increases faster than for illusory contours at low contrast.

4.4.6 Response degradation following a cortical injury

Lesions in V1 can be the result of contusions or cerebral vascular accidents (Trobe et al, 1973, Huber 1992). Their effect can be debilitating, and can cause a scotoma, which is an area of the visual field that can no longer be detected. Understanding the relationship between the extent of a lesion and its impact on the response of downstream neurons can be instrumental in optimally detecting and treating this condition. We used the model to characterize the changes in V2 cell responses to real and illusory contours following such a cortical injury.

The cortical lesion was simulated by rendering a number of V1 cells damaged (i.e., setting their firing rate to zero). The probability of a cell being damaged was

determined by a Gaussian distribution centered on the center of the lesion. The size of the lesion was determined by the standard deviation of the Gaussian. An image of a lesion corresponding to a standard deviation of 1 degree is shown superimposed on the orientation preference map in Figure 4.6.

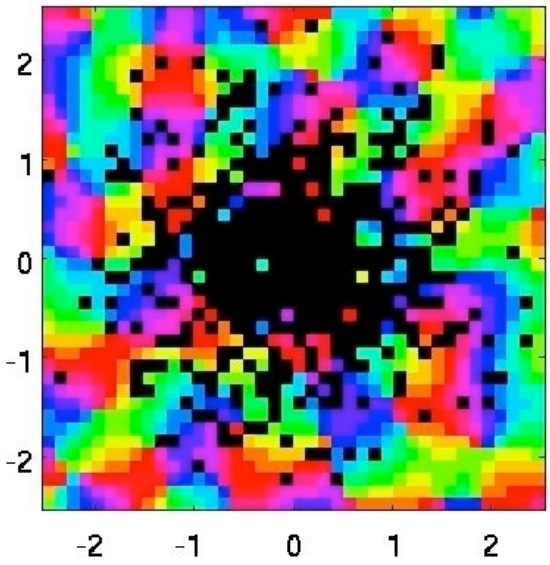

Figure 4.6 A lesion applied to complex cells in V1. The figure shows damaged cells (depicted by black dots) superimposed on the orientation map. The likelihood of a cell being damaged is based on a Gaussian probability. Twelve sizes of lesions are used, with sigma values ranging from 0.2 to 2.5 degrees. (σ is 1.0 for this image).

	Real Contours		Illusory Contours	
No Lesion	41.64	100%	26.54	100%
σ=0.2	38.42	92%	26.46	100%
σ=0.4	32.08	77%	23.33	88%
σ=0.6	24.98	60%	19.00	72%
σ=0.8	18.28	44%	14.49	55%
σ=1	13.72	33%	11.27	42%
σ=1.5	7.46	18%	5.76	22%
σ=2	2.86	7%	2.73	10%
σ=2.5	1.10	3%	1.52	6%

Table 2 Peak-to-trough height for real and illusory contour responses with lesions of various sizes

In order to assess the effect of a lesion on the ability of our model cortex to respond to contours, we looked at the tuning curves for full-field real and illusory contours as a function of lesion size. The first thing we observe is that as the size of the lesion increases, the tuning curves are scaled down while their half-width is maintained (figure not shown). Table 2 summarizes the peak to trough values for several sizes of lesions. The response to real contours degrades faster than the response to illusory contours (see also Figure 4.7). This effect is due to the greater contribution of the periphery of the pattern cell receptive field in the detection of illusory contours vs. real contours. The severity of a lesion centered on the center of the pattern cell receptive field will decrease towards the periphery of the receptive field; hence, the response to illusory

contours is less affected. For lesion sizes up to 1.1 degrees, the decrease in response is linear (Figure 4.7) and the slope is approximately 1.6 times greater for real contours than for illusory contours. For a lesion with a size of one degree, the response is ~33% of the original value for real contours, and ~42% of the original value for illusory contours. This means that information about the stimulus is still being transmitted from V1 to V2, which means that it could still be possible for the contour to be perceived.

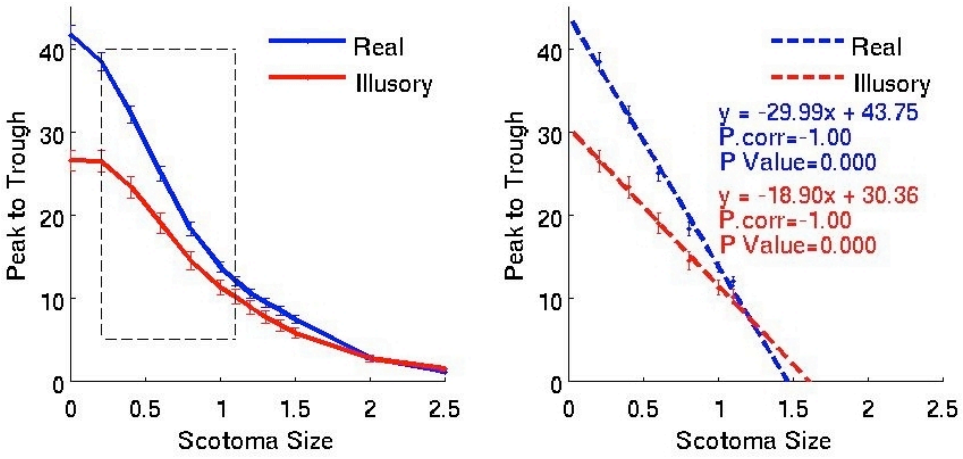

Figure 4.7 The effect of lesion size on the response to real and illusory contours. Left panel: Average peak to trough height of tuning curves for real (blue) and illusory (red) contours as a function of the size of the lesion. Right panel: Linear fit of peak to trough height as a function of lesion size for the area enclosed by the rectangle in left panel (lesion size σ=0.2 to σ=1.1).

4.5 Conclusion

4.5.1 Effect of the V1 orientation maps

One consequence of the fact that V1 is organized in orientation maps is that the

precision of the spatial sampling rate of orientations is limited by the size of the orientation domains relative to the range of likely connections (i.e. axonal projections and the size of the postsynaptic dendritic tree). The question that this raises is whether the effect of this limitation is large enough to invalidate the suggested mechanism for illusory contour detection. As our model shows, this is not the case: V2 cells in the model respond to both real and illusory contours. On the other hand, V1 orientation maps are source of significant variability in the amplitude of the tuning curves, while leaving the shape unchanged. Experimentally, variability in amplitude, tuning width, and peak have been recorded (Von der Heydt and Peterhans, 1989). This means that while orientation maps account for some of the variability observed in the amplitude of the tuning curves, they do not explain other variations in the tuning properties.

4.5.2 Origin of Inducer Spacing Preference

With respect to the dependence of response properties on inducer spacing, V2 cells can be grouped into two types: one type that exhibits inducer spacing preference and another that maintains approximately constant activity across a range of inducer spacings (Von der Heydt and Peterhans, 1989). Our results indicate that this dependence is related to the size of the receptive fields of presynaptic simple cells. More specifically, the first type can be explained by a narrow distribution of receptive field widths among pre-synaptic simple cells projecting to a given V2 neuron. The second type may be the result of a broader distribution of simple cell receptive field widths among pre-synaptic V1 neurons. Size considerations prevented us from fully testing the latter hypothesis, but

based on the shape of the individual curves corresponding to different receptive field widths it is plausible to assume that the combined input from several complex cells covering a range of spatial frequencies could provide the kind of inducer spacing invariance observed experimentally. Further modeling is necessary to confirm this.

4.5.3 Inducer Angle Dependence

Experimentally, a shift in the angle of the inducers relative to the illusory contour can either cause a shift of the orientation tuning curve towards the angle orthogonal to the inducer or leave the orientation tuning curve unaffected. This behavior can be explained by the distribution of the weights of different orientation preferences in the presynaptic input to the V2 cell. A shift in the tuning curve corresponds to pattern cells having their strongest synaptic connections to end-stopped cells of orthogonal preferred orientation, and much weaker synaptic connections to end-stopped cells of other preferred orientations. An invariant curve on the other hand corresponds to cells whose synaptic weights are only weakly dependent on the end-stopped cells' preferred orientations.

Experimentally, tracing synaptic connections with enough precision to determine which end-stopped cells are connected to particular pattern cells is a difficult challenge. While virus based retrograde labeling can label almost all presynaptic cells (Marshel et al. 2010), this technique does not yet allow for functional characterization. However, our hypothesis could be verified indirectly by constructing the tuning curve of a V2 neuron when the subject is first adapted to a grating with an orientation slightly shifted from the preferred orientation of the pattern cell. A shift in the tuning curve compared to the non-

adapted case would indicate that the pattern cells do indeed receive input from end-stopped cells with a range of orientation preferences, while the absence of such a shift would confirm that the majority of the synaptic input is provided by orthogonal end-stopped cells.

4.5.4 Contrast Response Function

The contrast response function for illusory contours generated by abutting gratings have rarely if ever been explored experimentally, for which reason there is no clear data to which we can compare our results. V2 cells in our model exhibited different contrast behavior when presented with illusory contours versus real contours, such that contrast response increased at a slower rate for illusory contours compared to real contours at low contrasts. Within the model this is due to the activation of end-stopped cells when an illusory contour is presented. Hence, an experimental measurement of this difference between the two contrast response functions would constitute a strong support for the hypothesis that end-stopped cells are fundamental for the detection of illusory contours.

4.5.5 Consequences of a V1 Lesion

V1 lesions can lead to visual impairments known as scotomas (Trobe et al, 1973, Huber 1992). Currently there is no clear consensus regarding the reversibility of such lesions. Some studies suggest that the injured area of the cortex never recovers any functionality (Bach-Y-Rita 1983, Balliet 1985, Pommerenke 1989), while other results

indicate that some degree of recovery is possible, seemingly driven by undamaged neurons in the lesioned area (Zihl 1981; Zihl and Cramon 1979; Kasten and Sabel 1995). In order to better understand the potential for recovery due to the remaining healthy neurons, it is necessary to first understand how large the effect of the lesion is on the downstream neurons. Our simulations show that the consequence of a small lesion (σ<1.1 degrees) is not an abrupt loss of response, but rather a gradual degradation in visual performance that increases linearly with size of the lesion. The consequence of this is that V2 neurons still respond to both real and illusory contour stimuli, albeit to a lesser degree. This allows for the possibility that a person with such a lesion could potentially recover the ability to detect contours in the damaged regions through strengthening of synaptic connections from healthy V1 neurons to V2 neurons in order to compensate for the diminished input. Such strengthening could potentially be achieved through targeted visual training (Zihl, 1981; Zihl and Cramon ,1979; Kasten and Sabel, 1995).

4.5.6 Further Consequences and Predictions

Due to the complexity of the proposed mechanism for illusory contour detection, in order to achieve a level of precision comparable to that achieved for real contours, the model had more V2 cells than V1 cells. Because area V2 is in fact smaller than area V1, the implication is that there must be a loss of precision in the detection of illusory contours compared with the detection of real contours. This loss of precision could occur in two ways. In one scenario, precision would be lost uniformly across the visual field, while in the other, precision would be similar for both types of contours at the level of

fovea but decrease for illusory contours at higher eccentricities. Which (if either) of these two scenarios is correct could be tested in a first approximation through psychophysics.

The first scenario can be tested using a "just noticeable differences" (JNDs) paradigm (Kingdom 2009), in which the subject signals whether there is a change in the position of the stimuli flashed successively two adjacent locations in the fovea. By comparing JNDs for illusory contours and real contours, it can be readily determined whether there is a loss of precision at the foveal level.

To test the second scenario, we need to determine the accuracy of illusory contour detection peripherally. This can be accomplished by measuring the ratio of correct identification of illusory contours inside full field collections of randomly arranged lines that occasionally form illusory contours at a random point in the visual field.

Chapter V

Effect of a cortical lesion on visual cognition

5.1 Introduction

Even relatively small lesions in the V1 area can lead to significant blind spots in the visual field of the subject. This condition is called a scotoma (cerebral blindness) and it has profound effects on visual perception. Historically, this condition has been considered permanent (Bach-Y-Rita 1983, Balliet 1985, Pommerenke 1989). However, in the past few decades, a significant body of evidence has accumulated indicating the contrary (Zihl et al 1977; Zihl and Cramon 1979; Zihl 1981; Kasten and Sabel 1995; Kasten 1998; Kasten 1999, Sabel 2000). This evidence points to two major means of vision restoration: spontaneous recovery and recovery through therapy. Spontaneous recovery depends on the underlying pathology and the extent of cerebral damage that is reversible. It takes place in the first few weeks following cortical injury. Generally, after 10-12 weeks, any further spontaneous recovery is negligible (Pambakian and Kennard 1997). Recovery through vision restoration therapy (VRT) is the result of several months of training during which spots of light are presented in the area of the visual field affected by the injury (Poggel et al. 2004). This recovery can take place even several years after

brain damage has occurred (Kasten 1998; Kasten 1999; Sabel 2000). The degree of recovery possible either via spontaneous recovery or using VRT is influenced by the shape of the scotoma. Evidence indicates that in the case of scotomas with sharp boundaries, only minimal recovery is possible, while for those with less distinct borders, there are significantly higher degrees of recovery (Teuber 1974; Zihl et al. 1977). Cortical plasticity is believed to play an important role in both spontaneous and training-induced recovery, but the underlying cortical mechanisms are still not fully understood. The task is made more difficult by the fact that visual perception is the result of several levels of processing, of which the primary visual cortex is one of the first. Hence, any model attempting to explain recovery would have to take into account this fact. To our knowledge, modeling attempts have been limited to predicting the outcome of the treatment based on existing treatment outcome benchmarks (Guenther 2009).

We propose a model that could explain both spontaneous and training-based vision recovery. The model is an extension of a firing rate model spanning visual processing from retina to V2 (see Chapter III) to which a new level corresponding to IT neurons has been added. This level is comprised of neurons able to detect depth ordering based on coincident alignment of unconnected line endings or edges. We used this model to study two distinct situations: A) spontaneous recovery occurs, and B) no spontaneous recovery occurs. In the first case, we found that if less than 60% of the cells providing input to the IT cell were damaged, recovery to pre-lesion levels could occur. For higher degrees of damage, some degree of recovery is also possible. In the second case, training-induced recovery can ameliorate visual performance by up to 80% as long as at least 60% of the cells providing input to the IT neuron are intact. When the RF of the IT

neuron is deeper into the scotoma, no improvement takes place through training. Based on these results, we advance the following hypotheses: A) spontaneous recovery is due to retraining of neurons downstream from the damaged area to the new activity patterns, and B) training-induced recovery is due to potentiation of existing synapses between undamaged neurons in the damaged area and downstream neurons.

5.2 The Model

Our model spans the ventral visual pathway from retina to IT and has two main components: a firing rate network (extending up to area V2) and a level corresponding to IT neurons that uses a support vector machine (SVM) approach to classify stimuli according to their depth ordering. The first component has been described in detail in section 3.2.

The second part of the model is comprised of 50 SVM units corresponding to IT neurons. Such units have been previously used to reproduce the behavior of neurons whose response is a result of supervised learning (Serre et al 2006, Serre et al 2007). In this model we follow the implementation from (Serre et al 2007). All IT neurons had the same V2 footprint of 5x5 degrees, each of them receiving input from 2^n neurons selected at random from their footprint. We explored configurations with values of n ranging from 1 to 9. Computationally, the SVMs were simulated using the LIBSVM library (Chang and Lin 2001). Supervised learning took place as follows: a randomly selected subset of distinct and unique stimuli consisting of 5% of total was used for testing, while the rest of

the stimuli were used for training. Performance of the classification was calculated as the percentage of correctly identified stimuli out of the total testing set. This operation was repeated 20 times to control for the possibility of a fortuitous choice of training and testing sets, and an average performance was calculated. The classification performance of the IT level was calculated as the population average of the performance of individual units. To calculate the performance level for the case in which the model only "guessed" the identity of the stimuli in the test (chance level) we used the same procedure as above, but with randomly assigned labels for the set of training stimuli.

5.3 Stimuli

The crossing stimuli consisted of overlapping dark vertical and bright horizontal bars at 100% contrast (Figure 5.1 A, B), with the vertical bar alternatively placed in the foreground ("vertical in front") or in the background ("vertical behind"). Both bars were full field length and 0.4 degrees in width. The vertical and horizontal bars could take any position along the horizontal and vertical axes, respectively, in increments of 0.2 degrees. We used a total of 1250 stimuli, 625 from each condition, evenly covering the 5x5 degrees of the visual field.

The non-crossing stimuli (Figure 5.1 C), used as control, consisted of a dark vertical bar flanked by two horizontal bright bars with one of them shifted vertically by 0.2 degrees with respect to the other, in order to render them non-collinear. The vertical and horizontal bars took the same positions as in the crossing stimuli case.

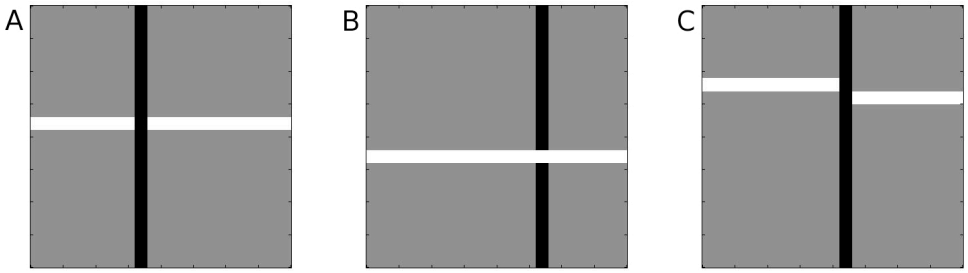

Figure 5.1 Stimuli used in figure-ground segregation task. The model was trained and tested on several stimuli, of the type A) vertical in front, B) vertical in back, and C) non-cross stimulus (used in the three-way classifier). 625 stimuli of each type were presented. In each case, the bars were 0.4 degrees in width, and they had vertical and horizontal orientations. All bars were full field. The stimuli varied only in the location of the cross (625 possible locations).

5.4 Results

5.4.1 Depth Ordering in the Healthy Cortex

We have previously shown that the first stage of the model (up to the V2 level) is capable of responding to both real and illusory contours, and that every level displays orientation and position tuning properties similar to those observed experimentally (see Chapter 3). Here we will show that the model is capable of performing a simple figure-ground separation task.

Figure 5.2 shows the performance of the model in correctly distinguishing between when the vertical bar is in the foreground versus when the vertical bar is in the background, as a function of the number of inputs from V2 neurons. The performance increases sharply until the number of inputs reaches 2^7, after which it saturates. This means that IT neurons can reach over 90% precision in background-separation task by

using input from approximately 8% of V2 neurons in their footprint.

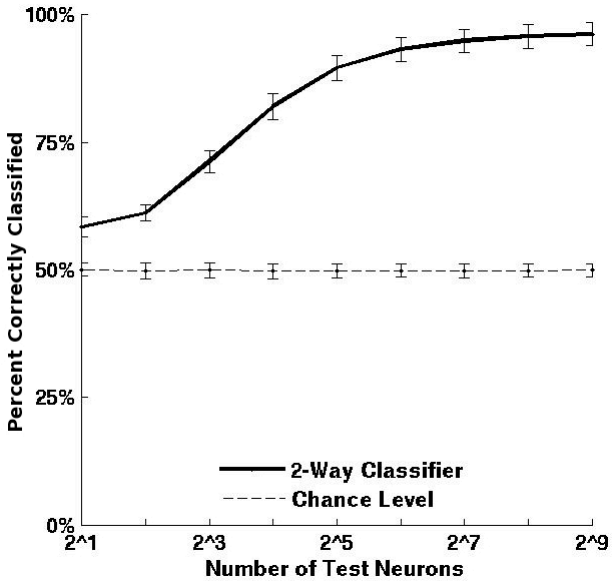

Figure 5.2 Classification performance of an IT unit in a 2-way classification task. The performance is shown as a function of the number of presynaptic neurons.

To control for the possibility that the model does not perform a figure – ground separation, but merely responds to the presence of horizontal bright bars and vertical dark bars in specific positions, we presented it with a set of stimuli in which crossing bars where mixed with non-crossing bars. If the second possibility was taking place, the model would be unable to make the distinction between the condition in which the vertical bar was in front and the non-crossing stimulus. Instead, the model correctly identified each type of stimulus in a 3-way classification task (Figure 5.3) with a performance level of up to 85% (against a chance level of 33%).

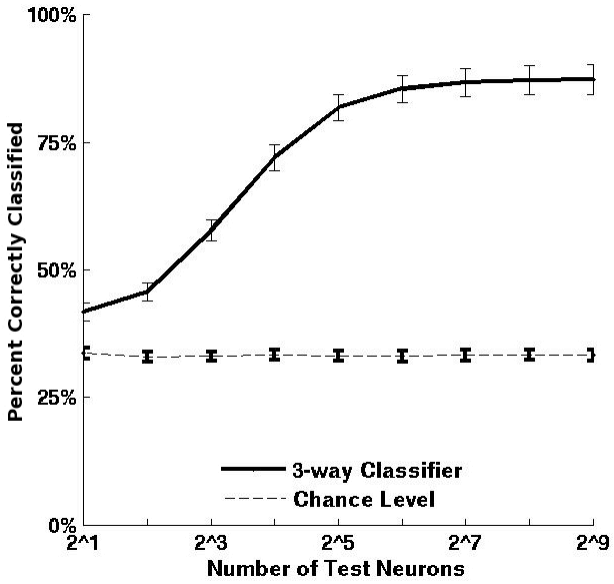

Figure 5.3 Classification performance of an IT unit in a 3-way classification task. The performance is shown as a function of the number of presynaptic neurons.

The ability of the model to correctly perform the task is due mainly to the presence of the excitatory complex cells. Indeed, removing the connections between end-stopped cells and pattern cells had only minor impact, while eliminating the connections between complex cells and pattern cells led to a sharp drop in classification performance regardless of the number of inputs, both in the case of the 2-way (Figure 5.4 A) and 3-way classifier (Figure 5.4 B).

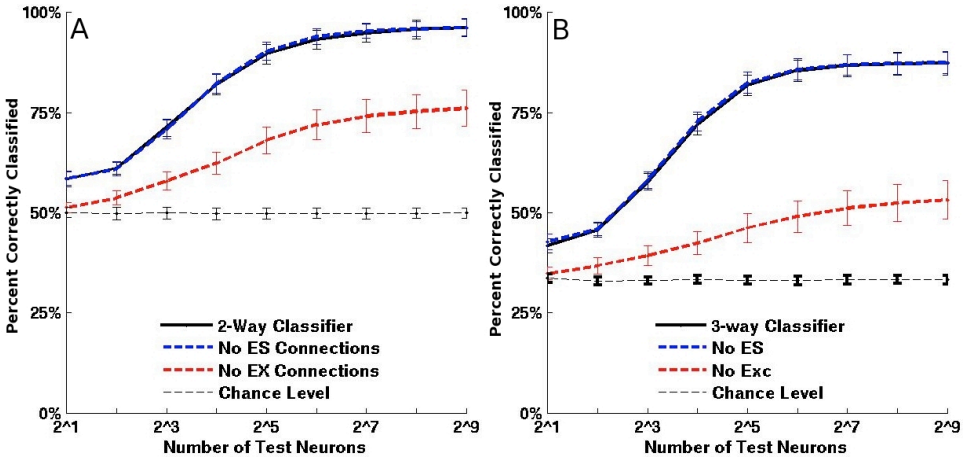

Figure 5.4 The importance of connections from V1 cell types. A) Performance of IT unit in a 2-way classification task in regular conditions (black curve), with no input from end-stopped cells (dotted blue curve), and with no input from complex cells (dotted red curve). B) Performance of IT unit in a 3-way classification task in regular conditions (black curve), with no input from end-stopped cells (dotted blue curve), and with no input from complex cells (dotted red curve). Note that performance degradation when input from complex cells is missing is significantly larger in a 3 way classification task.

5.4.2 Effect of a Lesion on Visual Performance

We examined the ability of the model to perform the figure-ground separation task when the V1 area is subject to lesions of various sizes. Such lesions are most often the consequence of an injury to the occipital area or a vascular accident (stroke), and can lead to extensive blind spots in the visual field (cerebral blindness). In the first few weeks after a lesion takes place, spontaneous recovery occurs in some cases. Receding inflammation and local healing of the injury is responsible for a large portion of the recovery, but some portion is likely due to cortical plasticity. In our model, we used lesions affecting between 25% and 95% of complex and end-stopped cells inside the footprint of the IT neurons (Figure 5.5). The lesion was centered on the visual field. The

probability that a neuron in the visual field would be damaged followed a normal distribution as a function of distance from the center of the visual field; a damaged neuron had its firing rate set to zero.

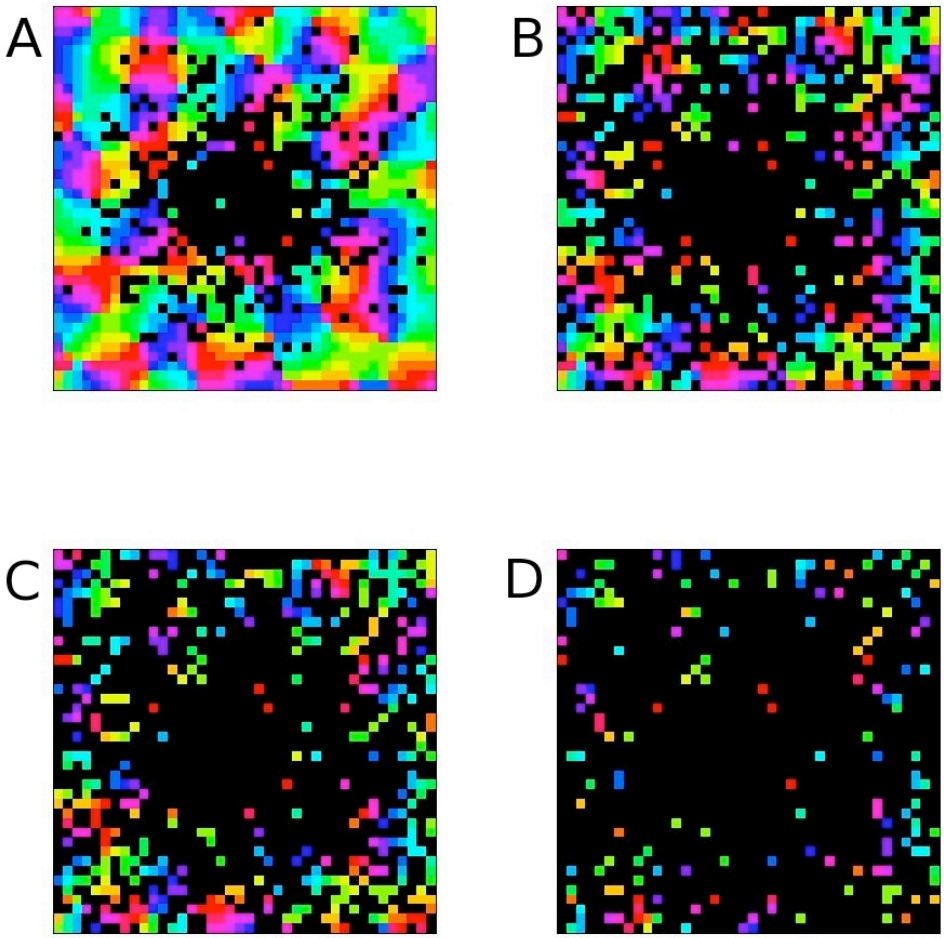

Figure 5.5 Examples of cortical injury in the model. Neurons are damaged with a probability following a normal distribution centered in the middle of the visual field. The images show lesions with A) 25% B) 63% C)73% and D) 90% damaged cells, superimposed on their orientation map.

First we estimated the effect of the lesion on cognitive performance before any

recovery takes place. This means that we looked at the post-lesion performance for the IT neurons that have already been trained using input from an undamaged V1. Figure 5.6 shows the performance of IT neurons in the figure-ground separation task as a function of the lesion size (solid line, number of inputs = 512 V2 neurons). From the point of view of performance degradation, there are two distinct cases. When the size of the lesion is less than 60% of the receptive field area, the performance is affected, but still significantly higher than chance level. When the size of the lesion is greater than 60% of the receptive field area, the performance drops sharply.

5.4.3 Spontaneous Recovery: Performance Improvement Through Pattern Relearning at the Level of IT Neurons

Some portion of the recovery that takes place beginning a few days post-injury can be attributed to cortical plasticity (Poggel et al, 2001; Tiel-Wilck and Kolmel, 1991). Currently it is unclear how much of the recovery is due to restoration of cell function following physical healing of the injury and how much of it is due to adaptive changes in synaptic strength and response patterns. In order to estimate the potential of recovery arising from the ability of neurons to adapt to new patterns of input, we retrained the IT neurons using the input from the injured cortex, and then tested them on stimuli presented to the injured cortex (Figure 5.6, dashed line). For cases in which fewer than 60% of cells presynaptic to the IT cell were damaged, performance was restored to levels close to pre-injury performance level. If more than 60% of presynaptic cells were damaged, full recovery no longer took place, but performance did increase significantly as long as there

were still undamaged neurons in the V2 area. This means that the ability of the IT neurons to learn can lead to substantial recovery in the days following the lesion, assuming that the IT neurons continue to receive input from the unharmed neurons in the visual area.

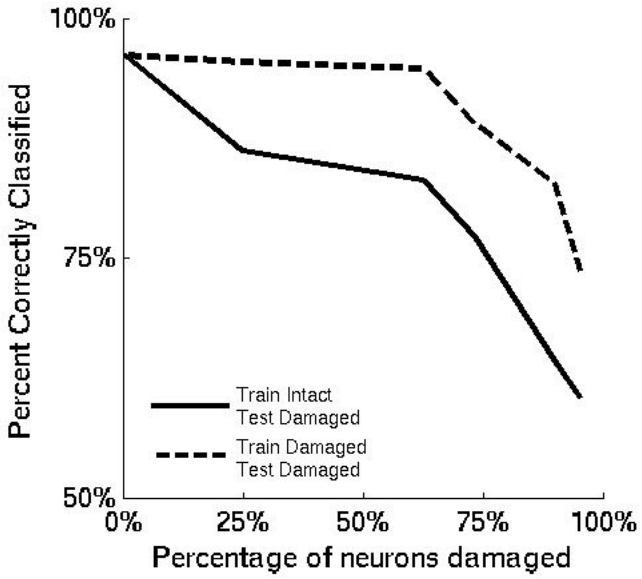

Figure 5.6 Potential for spontaneous recovery as a function of lesion size. Each IT unit has 512 (2^9) presynaptic inputs, and each point is the average response of 50 IT units. The solid line shows the performance of the IT unit when training is performed on the intact neurons and testing is performed on cells with presynaptic lesions. The dashed lines represent the performance when training and testing are both performed on the damaged cortex. This improves performance for all sizes of lesion, and improvement reaches levels near that of an undamaged cortex when fewer than 60% of the presynaptic complex cells are damaged.

5.4.4 Training Aided Recovery: Improvements Through Long Term Potentiation of Synapses Between Healthy Neurons in Lesion Area and Downstream Neurons

Historically it has been believed that the effects of a lesion were permanent once 10-12 weeks passed from the time of the injury. However, in the past two decades significant evidence has accumulated indicating that special training consisting of the presentation of visual stimuli in the blind spots of the visual field could reverse some of these effects. Such improvement in visual cognitive performance was attributed to the increase in the synaptic strength between the unharmed neurons in the lesion area and the downstream neurons. To investigate this possibility, we considered the situation of a lesion more than 10-12 weeks old, from which any possible spontaneous recovery has already taken place, and we explored the potential improvement in performance exclusively due to increased synaptic strength through long term potentiation. We simulated this by training the IT neurons using input from the healthy cortex, and then assessing their performance to stimuli presented to the damaged cortex (Figure 5.7) when the synaptic strength between the lesion area and the V2 area was a) normal (solid line), b) enhanced by up to 50% (dotted line), c) enhanced by up to 100% (dotted-dashed line) and d) enhanced by up to 200% (dashed line). We assumed a gaussian spatial LTP pattern, i.e. the maximum amplification took place for the connections from the V2 cells at the center of the receptive field. We found that when at least 40% of presynaptic cells were undamaged, performance increased by up to nearly 50%, but when more than 60% of cells were damaged, recovery was not possible.

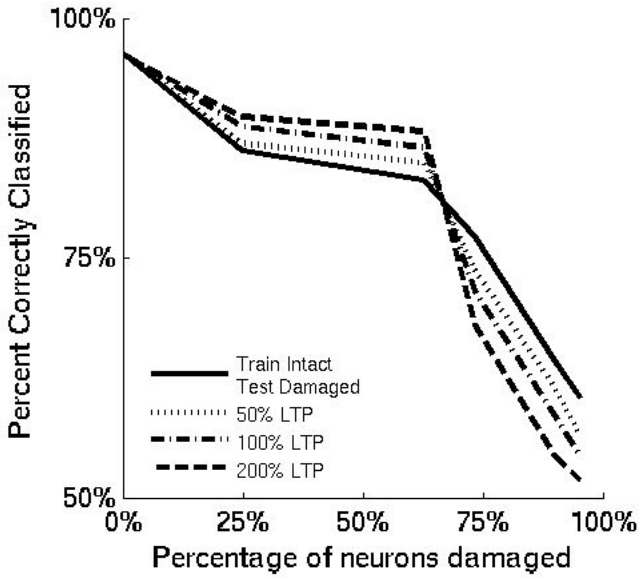

Figure 5.7 Potential for training-aided recovery as a function of lesion size. Each IT unit has 512 (2^9) presynaptic inputs, and each point is the average response of 50 IT units. The solid line shows the performance of the IT unit when training is performed on the intact neurons and testing is performed on cells with presynaptic lesions. The three dashed lines show the performance when the strength of synapses from complex cells to pattern cells is increased by 50%, 100% or 200%. This increases the performance when damage covers less than 60% of presynaptic cells.

5.4.5 Robustness to Noise

Information transmitted within the cortex is subject to a considerable amount of noise. One important question is whether the potential for recovery that we have observed is still possible when noise is present. To address this question, we applied 6 hz noise to the V1 simple cells in the form of a uniformly random input to each cell ranging between -3 and +3 hz, with an average value of 0 hz. This noise propagated to all downstream cell types.

We found that in the case of spontaneous recovery, performance is diminished

following the introduction of noise. Nevertheless, recovery still takes place for all sizes of lesions as long as less than 90% of the presynaptic neurons are damaged (Figure 5.8, left panel). Likewise, in the case of training-aided recovery, the addition of noise decreases performance, but recovery is still possible to some degree in cases where less than 60% of presynaptic cells are damaged (Figure 5.8, right panel). Based on these results we can conclude that the recovery mechanisms presented here remain valid even in the presence of noise.

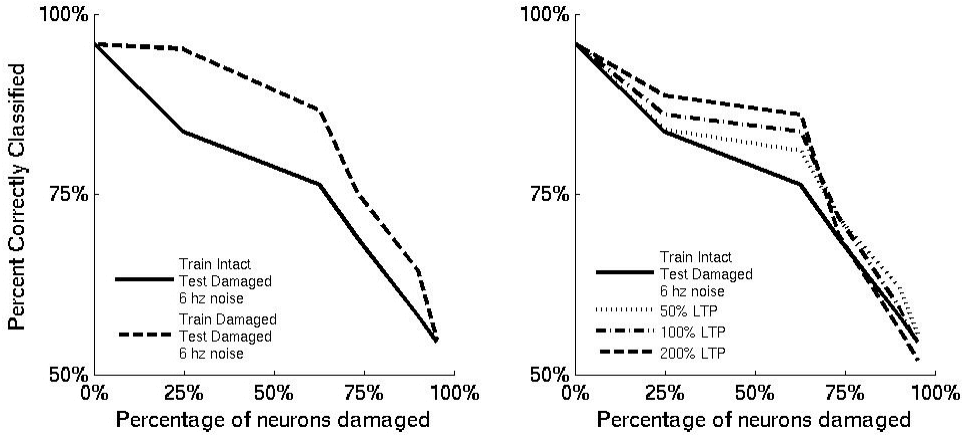

Figure 5.8 Spontaneous and training-aided recovery in the presence of noise. This figure shows the performance of an IT unit with 512 (2^9) inputs with the addition of 6 hz noise at the level of simple cells. The solid line in each panel shows the performance of the IT units when training is performed on the intact neurons and testing is performed on cells with presynaptic lesions. The dashed line in the left panel represent the performance when training and testing are both performed on the damaged cortex. In the right panel, the three dashed lines show the performance when the strength of synapses from complex cells to pattern cells is increased by 50%, 100% or 200%. In the case of spontaneous recovery (left panel), while the improvement in performance is lower after the addition of noise, recovery is still present for all lesion sizes affecting less than 90% of the presynaptic cells. Likewise, in the case of training-aided recovery (right panel), performance decreases after the addition of noise, but recovery is maintained when the lesion covers less than 60% of presynaptic complex cells.

5.5 Discussion

We have used a computational model capable of simulating simple visual perception functions such as elementary figure-ground separation to study the effects of cortical injuries in V1 area on visual cognition and the potential to recover functionality both immediately after the injury, and after a longer time period.

Early versus late recovery

In our model, recovery immediately following trauma takes place by retraining the downstream neurons in the extrastriate cortex to the new activity pattern of the neurons in the damaged area through a process of supervised learning. Recovery due to an older injury (more than 3 months) is modeled by strengthening the synapses between the neurons in the injured area and the post synaptic neurons in the extra striate cortex, through a long term potentiation process. We found that early recovery was more effective in restoring visual function: up to 80% improvement in performance on visual tasks versus a maximum of 50% improvement in the case of late recovery. This fact has important implications in the treatment strategies for patients suffering of hemianopia, as it suggests that training of visual functions has higher impact if applied early following an injury. Experimentally this conclusion could be tested through a series of psychophysical tests on a population of mice with localized injuries in area V1. The injury should be confined to one of the visual hemifields, and the mice should be split into two groups: a group receiving visual training and a control group. The mice in the "training" group will have the eye corresponding to the unaffected hemifield covered, in order to stimulate the usage of the neurons in the damaged area. After 3-4 weeks of training, the extent of visual function recovery will be tested in both groups. If our findings are correct, the group receiving remedial training will recover significantly more of the visual function than the control group.

The effect of the extent of the injury

The size of the damaged area relative to the footprint of the postsynaptic IT neuron emerged as an important quantity, as both loss and recovery of visual function followed a non-linear pattern. As long as at least 40% of the afferents neurons remained unaffected, significant functionality of the damaged area was preserved, and improvements were possible both through early and late recovery. When less than 40% of the neurons in the footprint of the IT neuron survived the injury, functionality was greatly reduced and early recovery was much less effective in visual restoration, while late recovery did not seem possible at all.

In conclusion, we showed that it is possible to use computational modeling as a practical tool in exploring realistic situations such the effect of cortical injury on visual function and potential for recovery.

Chapter VI

Discussion and Conclusion

6.1 Overview of Results

In this thesis, I present a model capable of illusory contour detection and its applications to current problems in neurobiology. The first application of the model was to study properties of V2 cells that respond to illusory contours. Although illusory contour detection has been studied extensively, there are still properties of illusory contour detecting cells that have not been explained. We have shown that illusory contour detection in V2 can be accomplished via a feed-forward mechanism using input from V1 cells arranged according to realistic orientation preference maps. Additionally, the arrangement of V1 cells in orientation maps can account in part for the variability in responses observed experimentally. We were also able to explain the following results at the single cell level for V2 cells that respond to illusory contours: 1) inducer spacing preference is dependent on the size of presynaptic cell receptive fields, 2) inducer angle dependence is based on the spectrum of orientation preferences in the presynaptic input, and 3) the contrast response function increases more slowly for illusory contours than for real contours.

Next we applied the model to the study of loss of visual perception following an injury in the V1 cortical area. V1 cortical injuries are debilitating, and while recovery does occur, the mechanisms behind it are still unclear. The purpose of the model was twofold: 1) to determine the relationship between the extent of the injury and the loss of visual functionality and 2) to investigate possible mechanisms of recovery. We found that for small injuries the degradation in response of neurons downstream from the injury area depended linearly on the size of the injury, leaving open the possibility of recovery of visual function. Based on this finding we evaluated two possible recovery mechanisms: spontaneous recovery, taking place in the first months following injury, and training-induced recovery that can be achieved even years later. We found that both mechanisms enable some degree of visual function restoration, but that spontaneous recovery is the most effective in regaining the maximum possible visual function.

6.2 Illusory Contour Detection: Model and Response of V2 cells

Illusory contours have been long used to study perceptual completion, but until 1984 these studies were carried out primarily at the psychophysical level. This changed when Von der Heydt et al. (1984) showed that neuronal correlates of illusory contours existed in cortical area V2 by recording responses to illusory contours from single cells. Over the next two decades, many other physiological investigations of illusory contours followed. Cells that respond to illusory contours have been recorded in cats (Zhan and Baker 2008, Sheth et al. 1996) and primates (Von der Heydt et al. 1984, Von der Heydt

and Peterhans 1989, Ramsden et al. 2001, Lee and Nguyen 2001), both in area V1 and area V2. Single unit responses to illusory contours have not been measured beyond area V2. Initial explanations for illusory contour detection were cognitive in nature, and emphasized top-down processes (Gregory 1972, Rock and Anson 1979). Later physiological results, however, supported a bottom-up approach based on successive feed-forward processes of increasing complexity. Consequently, several models explaining illusory contour detection have been advanced (Heitger et al. 1992; Heitger and von der Heydt 1993; Finkel and Edelman 1989; Grossberg and Mingolla 1985; Peterhans et al. 1986; Skrzypek and Ringer 1992; Ullman 1976). These models reproduce detection of illusory contours, but do not take into account topographic organization at the level of V1. Experimentally, orientation preference is mapped non-homogenously throughout V1, and it is not clear whether, with realistic topographic maps, detection would still be possible under these paradigms. Additionally, while these models are able to reproduce illusory contour detection at the population level, they are not able to reproduce or explain single cells responses, such as those recorded by Von der Heydt and Peterhans (1989).

Our model is an extension of the paradigm outlined by Heitger et al. (1992, 1998). The response to stimuli is built through successive computations in four stages, from simple cells to pattern cells, using feed-forward processes. Illusory contour detection is accomplished at the level of pattern cells. Unlike the model of Heitger et al. (1992, 1998), our model uses realistic topographic maps for all V1 cells. Our model proves that the mechanism laid out by Heitger et al (1992) can be used to achieve illusory contour detection even when realistic topographic orientation maps are used. Additionally, we

found that the response variability observed at the single cell level can be explained in part by the non-uniform distribution of orientation preferences at the level of V1. We used this model to investigate several response properties of single cells in area V2 that to date have not been explained. First, we looked at inducer spacing preference properties. Von der Heydt et al (1989) found two types of cells: one type that had a clear preference for a particular inducer spacing and another type that responded comparably across a range of inducer spacings. We found that inducer spacing preference is dependent on the size of the receptive fields of presynaptic inputs. Cells with a clear inducer spacing preference receive input from V1 cells with a narrow range of receptive field widths, while cells that do not show any dependence on inducer spacing receive input from V1 cells with a broad range of receptive field widths. Second, we analyzed the influence of the inducer angle. Experimentally, changing the orientation of the inducers relative to the illusory contour can cause a shift in the peak of the tuning curve, although the responses of some cells remain unaffected. Our model shows that the peak shift is characteristic of cells with a narrow spectrum of orientation preferences in the presynaptic input while a broad spectrum of orientations results in a response invariant to the relative inducer orientation. Finally, we modeled the contrast response function for illusory contours compared with real contours. To the best of our knowledge this has never been measured in a physiological experiment. We found that the contrast response function increases more slowly for illusory contours than for real contours, likely due to the additional processing step involving end-stopped cells.

Model limitations and future research

While the model is quite successful in reproducing illusory contour detection at the level of V2 and in explaining some of the single cell response properties, there are other experimental results that could not be accounted for using a feed-forward paradigm, such as the inverted responses at the level of V1 observed by Ramsden et al (2001) or the delayed responses in V1 measured by Lee and Nguyen (2001). Such results suggest the involvement of top down inputs to V1 from higher visual cortical areas. There is already significant evidence that feedback connections to V1 from higher cortical areas play an important role in visual attention, image recognition and image awareness (Ekstrom et al. 2008, Camprodon et al. 2009). Hence it would be natural that such connections also play a role in illusory contour detection. In order to take these effects into consideration, feedback connections should be added in the model between the V2 level and the V1 level. The addition of feedback connections will introduce additional complexities difficult to solve in a firing rate model, because timing will become important, as input from feedback connections arrives with a delay relative to feed-forward input

Another area for further research is the way information about illusory contours is encoded. Currently, in the model, the information is transmitted exclusively through a firing rate code. However, there is evidence that the visual cortex can perform tasks at very high speeds that are hard to reconcile with a purely firing rate based encoding system (Thorpe et al. 1996, Hung et al. 2005, Kirchner et al. 2006, Kirchner et al. 2009, Liu et al. 2009). To address this concern, a solution would be to translate the model into a spiking neuron model using the current schematic of cortical connections between the

different stages of the model. In order to do this, significant constraints imposed by computational resources limitations have to be overcome, as a spiking neuron model based on the current model would contain approximately 300,000 neurons, a prohibitively large number even for high-powered servers.

6.3 Cortical injuries: effect on visual function and ability to recover

V1 cortical injuries are debilitating, as they lead to scotomas, or blind spots in the visual field (Smith 1962, Huber 1992). Although historically this has been considered a permanent affliction, experimental and clinical results in the past two decades have accumulated an increasing body of evidence to the contrary. According to the recent research, restoration of visual function can take place both spontaneously and aided by special restorative training (Pambakian et al. 1997). The underlying neurological mechanism is yet not well understood, but it is believed to be related to cortical plasticity. Currently there is no model to help assess the relationship between the size of a cortical injury and its impact on visual function, nor is there a model to estimate the ability to recover. We address this problem using an enhanced version of the illusory contour detection model capable of performing simple figure-ground segregation tasks.

We first determined the relationship between the size of a V1 lesion and its effect on visual responses in higher cortical areas. We found that for small lesion sizes the response in downstream areas deteriorated linearly with the size of the lesion. When we

compared the effect on the detection of real and illusory contours, we found that, while the impact of a lesion increases as its size increases, this effect is less pronounced in the detection of illusory contours. This is due to the greater contribution of the periphery of the pattern cells receptive field to illusory contour responses.

Next we investigated the potential for the restoration of visual function both via spontaneous recovery and through training-induced recovery. We simulated the spontaneous recovery process by retraining the IT neurons on the new post-injury input patterns from the V2 pattern cells. Spontaneous recovery had the potential to enable full recovery of visual function if less than 60% of presynaptic cells were damaged. When the injured area was more extensive, some degree of recovery still occurred but full recovery was no longer possible. Recovery through restorative training was modeled as a strengthening of the synaptic connections between the remaining healthy V1 neurons in the injured area and the corresponding downstream V2 pattern cells. Training-induced recovery was less effective than spontaneous recovery in recovering functionality. While it provided up to 50% improvement of vision function when less than 60% of presynaptic cells were damaged, there was no possibility of recovery if the damage extended beyond 60% of presynaptic cells.

Model limitations and future research

In our approach to modeling the recovery of visual function we assumed that in the first few months after the injury the recovery was based purely on the retraining of downstream neurons to the new pattern of inputs, while past this period recovery was

based only on synaptic strengthening of the connections between the injured area in V1 and the downstream cells in area V2. In reality it is likely that the recovery is based on a mixture of both mechanisms, although currently available experimental and clinical data are not precise enough to clarify this aspect. In order to take both mechanisms into account simultaneously, a future version of the model should be able to gradually increase the synaptic strength between areas V1 and V2 while continually retraining the IT neurons to the new output patterns. Such an approach though would need prohibitive amounts of computation time due to the large set of stimuli used for training the IT units and would necessitate the use of large scale linux clusters.

6.4 Conclusions

We present several results based on a model capable of illusory contour detection. We first used the model to investigate properties of V2 cells that respond to illusory contours and found that a) detection of illusory contours via a feed-forward model can be accomplished using realistic topographic maps in V1, b) inducer spacing preference is determined by the receptive field width of presynaptic inputs, c) inducer angle dependence is dependent on the range of orientation preferences in the presynaptic input, and d) contrast response function increases more slowly for illusory contours than for real contours.

We then applied the model to the study of cortical injuries in V1 and found that a) deterioration of responses downstream from injured area increases linearly with the

extent of the damage for small injuries, b) spontaneous recovery can allow for full recovery if fewer than 60% of presynaptic cells are damaged, and c) training-induced recovery is less effective than the spontaneous recovery, and it can bring improvements of up to 50% if less than 60% of presynaptic input is damaged.

Taken together, these results show that computational modeling in neurobiology is not only a powerful tool for interpreting experimental results, it also provides solutions to current problems in medical and neurobiological research.

WORKS CITED

1. Ahmed, B., J. C. Anderson, K. A. C. Martin, and J. C. Nelson. "Map of the synapses onto layer 4 basket cells of the primary visual cortex of the cat." *Journal of Comparative Neurology* 380 (1997): 230-242.

2. Albright, T. D., and G. R. Stoner. "Contextual influences on visual processing." *Annual Review of Neuroscience* 25 (2002): 339-79.

3. Allman, John, Francis Miezin, and EveLynn McGuinness. "Direction- and velocity-specific responses from beyond the classical receptive field in the middle temporal visual area (MT)." *Perception* 14 (1985): 105-126.

4. Anzai, A., X Peng, and D. C. Van Essen. "Neurons in monkey area V2 encode combinations of orientations." *Nature Neuroscience* 10 (2007): 1313-1321.

5. Bach-Y-Rita, P. "Controlling variables eliminates hemianopia rehabilitation results." *Behaviroal and Brain Sciences* 6 (1983): 448.

6. Bair, Wyeth. "Spike timing in the mammalian visual system." *Current Opinion in Neurobiology* 9, no. 4 (1999): 447-453.

7. Balliet, R., K. M. T. Blood, and P. Bach-Y-Rita. "Visual field rehabilitation in the cortically blind?" *Journal of Neurology, Neurosurgery and Psychiatry* 48 (1985): 1113-24.

8. Bishop, P.O., J.S. Coombs, and G.H. Henry. "Receptive fields of simple cells in the cat striate cortex." *Journal of Physiology* 231 (1973): 31-60.

9. Blakemore, Colin, and Elisabeth A Tobin. "Lateral inhibition between orientation detectors in the cat's visual cortex." *Experimental Brain Research* 15, no. 4 (January 1972): 439-440.

10. Blasdel, G. G., and G. Salama. "Voltage sensitive dyes reveal a modular organization in monkey striate cortex." *Nature* 321 (1986): 579-85.

11. Bolz, J., and C. D. Gilbert. "Generation of end-inhibition in the visual cortex via interlaminar connections." *Nature* 320 (1986): 362-65.

12. Boser, B. E., I Guyon, and V. Vapnik. "A training algorithm for optimal margin classifiers." *Proceedings of the Fifth Annual Workshop on Comutational Learning Theory.* Pittsburgh: ACM Press, 1992. 144-152.

13. Bosking, W., Y. Zhang, B. Schofield, and D. Fitzpatrick. "Orientation selectivity and the arrangement of horizontal connections in tree shrew striate cortex." *Journal of Neuroscience* 17 (1997): 2112-2127.

14. Callaway, E. M. "Local cicrcuits in primary visual cortex of the macaque monkey ." *Annual Review of Neuroscience* 21 (1998): 47-74.

15. Callaway, E. M., and A. K. Wiser. "Contributions of individual layer 2–5 spiny neurons to local circuits in macaque primary visual cortex." *Visual Neuroscience* 13 (1996): 907-922.

16. Camprodon, Joan A., Ehud Zohary, Verena Brodbeck, and Alvaro Pascual-Leone. "Two Phases of V1 Activity for Visual Recognition of Natural Images." *Journal of Cognitive Neuroscience* 22 (2010): 1262-9.

17. Chance, F. S., S. B. Nelson, and L. F. Abbott. "Complex cells as cortically amplified simple cells." *Nature Neuroscience* 2 (1999): 277-282.

18. Chang, Chih-Chung, and Chih-Jen Lin. *LIBSVM : a library for support vector machines.* 2001. http://www.csie.ntu.edu.tw/~cjlin/libsvm.

19. Cortes, C., and V. Vapnik. "Support-vector network." *Machine Learning* 20 (1995): 273-297.

20. Dayan, P., and L. F. Abbott. Theoretical neuroscience: computational and mathematical modeling of neural systems. Cambridge, MA: The MIT Press, 2001.

21. De Valois, R. L., L. G. Thorell, and D. G. Albrecht. "Periodicity of striate-cortex-cell receptive fields." *Journal of the Optical Society of America A* 2 (1985): 1115-1123.

22. Ekstrom, Leeland B., Pieter R. Roelfsema, John T. Arsenault, Giorgio Bonmassar, and Wim Vanduffel. "Bottom-Up Dependent Gating of Frontal Signals in Early Visual Cortex." *Science* 321 (2008): 414-417.

23. Felleman, D.J ., and D. C. Van Essen. "Distributed Hierarchical Processing in the Primate Cerebral Cortex." *Cerebral Cortex* 1 (1991): 1-47.

24. Field, D. J., and D. J. Tolhurst. "The Structure and Symmetry of Simple-Cell Receptive-Field Profiles in the Cat's Visual Cortex." *Proceedings of the Royal Society of London B* 228 (1986): 379-400.

25. Finkel, L. H., and G. M. Edelman. "Integration of distributed cortical systems by reentry: a computer simulation of interactive functionally segregated visual areas." *Journal of Neuroscience* 9 (1989): 3188-3208.

26. Fitzpatrick, D., J. S. Lund, and G. G. Blasdel. "Intrinsic connections of macaque striate cortex: afferent and efferent connections of lamina 4C." *Journal of Neuroscience* 5 (1985): 3329-3349.

27. Gilbert, C. D. "Laminar differences in receptive field properties of cells in cat primary visual cortex." *Journal of Physiology* 268 (1977): 391-421.

28. Gilbert, C. D., and J. P. Kelly. "The projections of cells in different layers of the cat's visual cortex ." *Journal of Comparative Neuroloby* 163 (1975): 81-106.

29. Girard, P., P. A. Salin, and J. Bullier. "Response selectivity of neurons in area MT of the macaque monkey during ververs ible inactivation of area V1." *Journal of Neurophysiology* 67 (1992): 1437-46.

30. Goodale, Melvyn A, and A. David Milner. "Separate visual pathways for perception and action." *Trends in Neurosciences* 15, no. 1 (January 1992): 20-25.

31. Gregory, R. L. *Nature* 238 (1972): 51-52.

32. Grinvald, A., E Lieke, R. D. Frostig, C. D. Gilbert, and Wiesel T. N. "Functional architecture of cortex revealed by optical imaging of intrinsic signals." *Nature*, 1986: 361-4.

33. Gross, C. G., C. E. Rocha-Miranda, and B. Bender. "Visual properties of neurons in inferotemporal cortex of the Macaque." *Journal of Neurophysiology* 35 (1972): 96-111.

34. Grossberg, S., and E. Mingolla. "Neural dynamics of perceptual grouping: Textures, boundaries, and emergent segmentations." *Perception and Psychophysics* 38 (1985): 141-171.

35. Heggelund, P. "Quantitative studies of the discharge fields of single cells in cat striate cortex." *Journal of Physiology (London)* 373 (1986): 217-292.

36. Heggelund, P., and K. Albus. "Response variability and orientation discrimination of single cells in striate cortex of cat." *Experimental Brain Research* 32 (1978): 197-211.

37. Heitger, F., and R. von der Heydt. "A computational model of neural contour processing: figure-ground segregation and illusory contours." *Proc. 4th Int. Conf. Computer Vision*, 1993: 32-40.

38. Heitger, F., L. Rosenthaler, R. von der Heydt, E. Peterhans, and O. Kübler. "Simulation of Neuron Contour Mechanisms from Simple to End-stopped Cells." *Vision Research* 32 (1992): 963-982.

39. Heitger, F., R. von der Heydt, E. Peterhans, L. Rosenthalerd, and O. Kiibler. "Simulation of neural contour mechanisms: representing anomalous contours." *Image and Vision Computing* 16 (1998): 407-421.

40. Hirsch, J. A., and C. D. Gilbert. "Synaptic physiology of horizontal connections in the cat's visual cortex." *Journal of Neuroscience* 11 (1991): 1800-1809.

41. Hollander, H. "On the origins of corticotectal projections in the cat." *Experimental Brain Research* 21 (1974): 430-440.

42. Hollander, H. "The projection from the visual cortex to the lateral geniculate body (LGB). An experimental study with silver impregnation methods in the cat." *Experimental Brain Research* 21 (1970): 430-440.

43. Hubel, D. H., and T. N. Wiesel. "Laminar and columnar distribution of geniculo-cortical fibres in the macaque monkey." *Journal of Comparative Neurology* 146 (1972): 421-450.

44. Hubel, D. H., and T. N. Wiesel. "Receptive Fields and Functional Architecture in two Nonstriate Areas (18 and 19) of the Cat." *Journal of Neurophysiology* 28 (1965): 229-289.

45. Hubel, D. H., and T. N. Wiesel. "Receptive fields, binocular interaction and functional architecture in the cat's visual cortex." *Journal of Physiology* 160 (1962): 106-154.

46. Hubel, D. H., and T. N. Wiesel. "Sequence regularity and geometry of orientation columns in the monkey striate cortex." *Journal of Comparative Neurology* 158 (1974): 267-294.

47. Hubel, D. H., T. N. Wiesel, and M. P. Stryker. "Anatomical Demonstration of Orientation Columns in Macaque Monkey." *Journal of Comparative Neurology* 177 (1978): 361-80.

48. Hubel, David. *Eye, Brain and Vision.* New York: Scientific American Library, 1995.

49. Hubel, David H, and Torsten N Wiesel. "Integrative action in the cats lateral geniculate body." *Journal of Physiology* 155 (1961): 385-398.

50. Hubel, David H, and Torsten N Wiesel. "Receptive fields, binocular interaction and functional architecture in the cat's visual cortex." *Journal of Physiology* 162 (1962): 106-154.

51. Huber, A. "Homonymous hemianopia." *Neuro-opthalmology* 12 (1992): 351-66.

52. Huber, A. "Homonymous hemianopia, a review of one hundred cases." *American Journal of Opthalmology* 54 (1992): 616-23.

53. Hung, Chou P., Gabriel Kreiman, Tomaso Poggio, and James J. DiCarlo. "Fast Readout of Object Identity from Macaque Inferior Temporal Cortex." *Science* 310 (2005): 863-866.

54. Jones, J. P., and L. A. Palmer. "An Evaluation of the Two-Dimensional Gabor Filter Model of Simple Receptive Fields in Cat Striate Cortex." *Journal of Neurophysiology* 58 (1987): 1233-1258.

55. Kandel, Eric, James Schwartz, and Thomas Jessell. *Principles of Neural Science.* McGraw Hill Medical, 2000.

56. Kasten, E., D. A. Poggel, E. M. Müller-Oehring, J. Gothe, T. Schulte, and B. A. Sabel. "Restoration of vision II: residual functions and training-induced visual field enlargement in brain-damaged patients." *Restor Neurol Neurosci* 15 (1999): 273-287.

57. Kasten, E., S. Wüst, and Sabel, B. A. Behrens-Baumann W. "Computer-based training for the treatment of partial blindness." *Nature Medicine* 4 (1998): 1083-1087.

58. Katsen, E., and B. A. Sabel. "Visual field enlargement after computer training in brain-damaged pationes with homonymous deficits: an open pilot trial." *Rest. Neurol. Neurosci.* 8 (1995): 113-127.

59. Katzner, S., L. Busse, and M. Carandini. "GABAA Inhibition Controls Response Gain in Visual Cortex." *Journal of Neuroscience* 31 (2011): 5931-41.

60. Kawamura, S, J. M. Sprague, and K Niimi. "Corticofugal Projections from the Visual Cortices to the Thalamus, Pretectum and Superior Colliculus in the Cat." *Journal of Comparative Neurology* 158, no. 339 (1974): 362.

61. Kingdom, F. Psychophysics: A Practical Introduction. Academic Press, 2009.

62. Kirchner, H, and SJ Thorpe. "Ultra-rapid object detection with saccadic eye movements: visual processing speed revisited." *Vison Research* 46 (2006): 1762-1776.

63. Kirchner, Holle, Emmanuel J. Barbeau, Simon J. Thorpe, Jean Regis, and Catherine Liegeois-Chauvel. "Ultra-Rapid Sensory Responses in the Human Frontal Eye Field Region." *The Journal of Neuroscience* 29, no. 23 (2009): 7599-7606.

64. Kohonen, T. "Self-organized formation of topologically correct feature maps." *Biological Cybernetics* 43 (1982): 59-69.

65. Kuffler, Stephen W. "DISCHARGE PATTERNS AND FUNCTIONAL ORGANIZATION OF MAMMALIAN RETINA." *Journal of Neurophysiology* 13 (1953): 37-68.

66. Kuffler, Stephen W. "Neurons in the retina: Organization, inhibition and exctiatory problems." *Cold Spring Harbor on Quantitative Biology* 17 (1952): 281-292.

67. Lee, T. S., and M. Nguyen. "Dynamics of Subjective Contour Formation in the Early Visual Cortex." *PNAS*, 2001: 1907-1911.

68. LeVay, S., and C. D. Gilbert. "Laminar patterns of geniculocortical projection in the cat ." *Brain Research* 113 (1976): 1-19.

69. Liu, H., Y. Agam, J.R. Madsen, and G. Kreiman. "Timing, timing, timing: fast decoding of object information from intracranial field potentials in human visual cortex." *Neuron* 62, no. 2 (2009): 281-90.

70. Maffei, L, and A Fiorentini. "The unresponsive regions of visual cortical receptive fields." *Vision Research* 16 (1976): 1131--l139.

71. Marshel, J. H., T. Mori, K. J. Nielsen, and E. M. Callaway. "Targeting Single Neuronal Networks for Gene Expression and Cell Labeling In Vivo." *Neuron* 67 (2010): 562–574.

72. McCormick, David A, Barry W Connors, and James W Lighthall. "Comparative electrophysiology of pyramidal and sparsely spiny stellate neurons of the neocortex." *Journal of Neurophysiology* 54, no. 4 (1985): 782-806.

73. McGuire, B. A., C. D. Gilbert, P. K. Rivlin, and T. N. Wiesel. "Targets of horizontal connections in macaque primary visual cortex ." *Journal of Comparative Neurology* 305 (1991): 370-392.

74. McGuire, B. A., J. P. Hornung, C. D. Gilbert, and T. N. Wiesel. "Patterns of synaptic input to layer 4 of cat striate cortex." *Journal of Neuroscience* 4 (1984): 3021-3033.

75. Morrone, M. C., D. C. Burr, and L. Maffei. "Functional implication of cross-orientation inhibition of cortical visual cells. I. Neurophysiological evidence." *Proceedings of the Royal Society of London, Series B* 216 (1982): 335-354.

76. Movshon, J. A., I. D. Thompson, and D. J. Tolhurst. "Nonlinear spatial summation in the receptive fields of complex cells in the cat striate cortex." *Journal of Physiology* 283 (1978): 78–100.

77. Nelson, J. I., and B. J. Frost. "Orientation-selective inhibition from beyond the classic visual receptive field." *Brain Research* 139 (1978): 359-365.

78. Nieder, A. "Seeing more than meets the eye: processing of illusory contours in animals." *Journal of Comparative Physiology A* 188 (2002): 249-260.

79. Orban, Guy A., H. Kato, and P.O. Bishop. "Dimension and properties of end-zone inhibitory areas in receptive fieIds of hyper- complex cells in cat striate cortex." *Journal of Neurophysiology* 42 (1979): 833-849.

80. Palmer, L. A., and A. C. Rosenquist. "Visual receptive fields of single striate cortical units projecting to the superior colliculus in the cat ." *Brain Research* 67 (1974): 27-42.

81. Palmer, L. A., and T. L. Davis. "Receptive-field structure in cat striate cortex." *Journal of Neurophysiology* 46 (1981): 260-276.

82. Pambakian, A. L. M., and C. Kennard. "Can visual function be restored in patients with homonymous hemianopia?" *British Journal of Opthalmology* 81 (1997): 324-328.

83. Pei, X., T. R. Vidyasagar, M. Volgushev, and O. D. Creutzfeldt. "Receptive field analysis and orientation selectivity of postsynaptic potentials of simple cells in cat visual cortex." *Journal of Neuroscience* 14 (1994): 7130-7140.

84. Peterhans, E., R. von der Hedyt, and G. Baumgartner. "Neuronal responses to illusory contour sitimuli reveal stages of visual cortical processing." *Visual Neuroscience*, 1986: 343-351.

85. Pillow, J., and N. Rubin. "Perceptual completion across the vertical meridian and the role of early visual cortex." *Neuron* 33 (2002): 805-813.

86. Poggel, D. A., E Kasten, and B. A. Sabel. "Attentional cueing improves vision restoration therapy in patients with visual field defects." *Neurology* 63 (2004): 2069-2076.

87. Poggel, D. A., E. Kasten, E. M. Müller-Oehring, B. A. Sabel, and S. A. Brandt. "Unusual spontaneous and training induced visual field recovery in a patient with a gunshot lesion." *J Neurol Neurosurg Psychiartry* 70 (2001): 236-239.

88. Pollen, D. A., and S. F. Ronner. "Spatial Computation Performed by Simple and Complex Cells in the Visual Cortex of the Cat." *Vision Research* 22 (1982): 101-118.

89. Pommerenke, K., and H. J. Markowitsch. "Rehabilitation training of homonymous visual field defects in patients with postgeniculate damage of the visual system." *Restorative Neurology and Neuroscience* 1 (1989): 47-63.

90. Ringach, D. L. "Spatial structure and symmetry of simple-cell receptive fields in macaque primary visual cortex." *Journal of Neurophysiology* 88 (2002): 455-463.

91. Ringach, D. L., R. M. Shapley, and M. J. Hawken. "Orientation Selectivity in Macaque V1: Diversity and Laminar Dependence." *The Journal of Neuroscience* 22 (2002): 5639-5651.

92. Rock, I., and R. Anson. "Illusory contours as the solution to a problem." *Perception* 8 (1979): 665-681.

93. Rodman, H. R., C. G. Gross, and T. D. Albright. "Afferent basis of visual response properties in area MT of the macaque. I. Effects of striate cortex removal." *Journal of Neuroscience* 2 (1989): 2033-50.

94. Sabel, B. A. "Restoration of vision I: neurobiological mechanisms of restoration and plasticity after brain damage– a review." *Restor Neurol Neurosci* 15 (1999): 177-200.

95. Sabel, B. A., and E. Kasten. "Restoration of vision by training of residual functions." *Current Opinion in Opthalmology* 11 (2000): 430-436.

96. Schmidt, K. E., R. Goebel, S. Löwel, and W. Singer. "The perceptual grouping criterion of colinearity is reflected by anisotropies of connections in the primary visual cortex ." *European Journal of Neuroscience* 9 (1997): 1083-1089.

97. Shepherd, Gordon. *Creating Modern Neuroscience:The Revolutionary 1950s.* New Yrok: Oxford University Press, 2009.

98. Sheth, B. R., J. Sharma, S. C. Rao, and M. Sur. "Orientation Maps of Subjective Contours in Visual Cortex." *Science* 274 (1996): 2110-2115.

99. Sincich, L. C., Park K. F., M. J. Wohlgemuth, and Horton J. C. "Bypassing V1: A direct geniculate input to area MT." *Nature Neuroscience* 7 (2004): 1123-8.

100. Skrzypek, J., and B. Ringer. "Neural network models for illusory contour perception." *Proc. CVPR*, 1992: 586-591.

101. Smith, J.L. "Homonymous hemianopia, a review of one hundred cases." *Americal Journal of Opthalmology* 54 (1962): 616-23.

102. Somers, D. C., S. B. Nelson, and M. Sur. "An emergent model of orientation selectivity in cat visual cortical simple cells." *The Journal of Neuroscience* 15 (1995): 5448-5465.

103. Stratford, K. J., K. Tarczy-Hornoch, K. A. C. Martin, N. J. Bannister, and J. J. B. Jack. "Excitatory synaptic inputs to spiny stellate cells in cat visual cortex." *Nature* 382 (1996): 258-261.

104. Tamas, G., P. Somogyi, and E. H. Buhl. "Differentially interconnected networks of GABAergic interneurons in the visual cortex of the cat." *Journal of Neuroscience* 18 (1998): 4255-4270.

105. Teuber, H. L. "Recovery of function after lesions of the central nervous system: history and postretinal lesions." *Experimental Brain Research* 27 (1974): 245-249.

106. Thorpe, Simon, Denis Fize, and Catherine Marlot. "Speed of processing in the human visual system." *Nature* 381 (1996): 520-522.

107. Tiel-Wilck, K, and H. W. Kölmel. "Patterns of recovery from homonymous hemianopias subsequent to infarction in the distribution of the posterior cerebral artery." *Neuroopthalmology* 11 (1991): 33-39.

108. Toyama, K., K. Matsunami, T. Ohno, and S. Takashiki. "An intracellular study of neuronal organization in the visual cortex." *Experimental Brain Research* 21 (1974): 45-66.

109. Trobe, J. D., M. L. Lorber, and N. S. Schlezinger. "Isolated homonymous hemianopia: A review of 104 cases." *Arch Opthalmol* 89 (1973): 377-81.

110. Ts'o, D. Y., R. D. Frostig, E. E. Lieke, and A. Grinvald. "Functional organization of primate visual cortex revealed by high resolution optical imaging." *Science* 249 (1990): 417-420.

111. Ullman, S. "Filling-in the gaps: The shape of subjective contours and a model for their generation." *Biological Cybernetics* 25 (1976): 1-6.

112. Updyke, B. V. "The Patterns of Projection of Cortical Areas 17, 18, and 19 onto the Laminae of the Dorsal Lateral Geniculate Nucleus in the Cat." *Journal of Comparative Neurology* 163 (1975): 377-396.

113. Von der Heydt, R., and E. Peterhans. "Mechanisms of Contour Perception in Monkey Visual Cortex. I. Lines of Pattern Discontinuity." *Journal of Neuroscience* 9 (1989): 1731-48.

114. Von der Heydt, R., E. Peterhans, and G. Baumgartner. "Illusory contours and cortical neuron responses." *Science* 224 (1984): 1260-1262.

115. Zhan, C. A., and C. L. Baker. "Critical Spatial Frequencies for Illusory Contour Processing in Early Visual Cortex." *Cerebral Cortex* 18 (2008): 1029-1041.

116. Zihl, J. "Recovery of visual functions in patients with cerebral blindness: Effect of specific practice with saccadic localization." *Experimental Brain Research* 44 (1981): 159-169.

117. Zihl, J., and D. Y. von Cramon. "Restitution of visual field function in patients with cerebral blindness." *J. Neurol Neurosurg. Psychiat.* 42 (1979): 312-32.

118. Zihl, J., D. von Cramon, R. Brinkmann, and H. Backmund. "The course and prognosis of scotomas in patients with cerebrovascular disorders." *Nervenarzt* 48 (1977): 219-224.